



Research paper

From dual binding site acetylcholinesterase inhibitors to allosteric modulators: A new avenue for disease-modifying drugs in Alzheimer's disease



Talita P.C. Chierrito ^a, Susimaire Pedersoli-Mantoani ^a, Carlos Roca ^b, Carlos Requena ^b, Victor Sebastian-Perez ^b, Willian O. Castillo ^c, Natalia C.S. Moreira ^c, Concepción Pérez ^e, Elza T. Sakamoto-Hojo ^{c,d}, Catarina S. Takahashi ^{c,d}, Jesús Jiménez-Barbero ^{b,f}, F. Javier Cañada ^b, Nuria E. Campillo ^b, Ana Martinez ^{b,**}, Ivone Carvalho ^{a,*}

^a School of Pharmaceutical Sciences of Ribeirão Preto, University of São Paulo, Avenida do Café, s/n, 14040-903, Ribeirão Preto, SP, Brazil

^b IPSBB Unit, Centro de Investigaciones Biológicas (CSIC), Ramiro de Maeztu 9, 28040 Madrid, Spain

^c Department of Genetics, Ribeirão Preto Medical School, University of São Paulo, Av. Bandeirantes, 3900, 14049-900, Ribeirão Preto, SP, Brazil

^d Department of Biology, Faculty of Philosophy, Sciences and Letters at Ribeirão Preto, University of São Paulo, Avenida Bandeirantes, 3900, 14040-900, Ribeirão Preto, SP, Brazil

^e Instituto de Química Médica (CSIC), Juan de la Cierva 3, 28006, Madrid, Spain

^f CIC BioGUNE, Parque Tecnológico de Bizkaia, Edif. 801A, 48160, Derio-Bizkaia, Bilbao, Spain

ARTICLE INFO

Article history:

Received 6 July 2017

Received in revised form

21 August 2017

Accepted 22 August 2017

Available online 26 August 2017

Keywords:

Acetylcholinesterase inhibitors

Allosteric modulators

Alzheimer's disease

ABSTRACT

The lack of an effective treatment for Alzheimer's disease (AD), an increasing prevalence and severe neurodegenerative pathology boost medicinal chemists to look for new drugs. Currently, only acetylcholinesterase (AChE) inhibitors and glutamate antagonist have been approved to the palliative treatment of AD. Although they have a short-term symptomatic benefits, their clinical use have revealed important non-cholinergic functions for AChE such its chaperone role in beta-amyloid toxicity. We propose here the design, synthesis and evaluation of non-toxic dual binding site AChEIs by hybridization of indanone and quinoline heterocyclic scaffolds. Unexpectedly, we have found a potent allosteric modulator of AChE able to target cholinergic and non-cholinergic functions by fixing a specific AChE conformation, confirmed by STD-NMR and molecular modeling studies. Furthermore the promising biological data obtained on human neuroblastoma SH-SY5Y cell assays for the new allosteric hybrid **14**, led us to propose it as a valuable pharmacological tool for the study of non-cholinergic functions of AChE, and as a new important lead for novel disease modifying agents against AD.

© 2017 Elsevier Masson SAS. All rights reserved.

1. Introduction

Firstly described as an "unusual disease of the cerebral cortex" in 1906 [1], Alzheimer disease (AD) is a neurodegenerative disorder characterized by a slow, silent and progressive damage of the human brain that remains uncured and fatal. The first signals of AD are memory failure and cognitive impairment, which progresses to memory loss and behavioral changes [2,3]. The underlying

mechanisms include cholinergic transmission decreasing, abnormal processes as beta-amyloid ($A\beta$) deposits and neurofibrillary tangles due hyperphosphorylation of tau protein. In 2015, it was estimated that there were 46.8 million people worldwide with dementia, affecting mainly those over the age 65. This number will reach around 131.5 million in 2050 [4].

The treatments for mild-moderate AD are based on drugs that boost the levels of acetylcholine by inhibiting acetylcholinesterase (AChE), such as donepezil, galantamine, rivastigmine and tacrine, the latter no longer prescribed due its hepatotoxicity, as well as the NMDA receptor antagonist, memantine, for severe AD. Although acetylcholinesterase inhibitors (AChEIs) are not able to halt the progress of the disease, these drugs improve the quality of life for patients and caregivers [5]. Furthermore, evidence has indicated

* Corresponding author.

** Corresponding author.

E-mail addresses: ana.martinez@csic.es (A. Martinez), [\(I. Carvalho\).](mailto:carronal@usp.br)

that some of these acetylcholinesterase inhibitors also have non-cholinergic functions on the pathogenesis of AD [6].

The symptomatic short-term benefits of AChEIs led to new therapeutic strategies focused on amplifying the cholinergic activity at M-1 muscarinic and α -7 nicotinic receptors, as illustrated by cevimeline and encencline (EVP-6124), respectively [7]. Also of upmost importance is the modulation of enzymes involved in the proteolytic cleavage of the amyloid precursor protein (APP) owing to the $A\beta_{(1-42)}$ metabolite neurotoxicity in senile plaques formation and soluble oligomeric $A\beta$ deposits [8]. In this regard, the inhibition of BACE-1 (β -secretase) has been highly explored, leading to verubecestat (MK8931) [9] in clinical trials. In addition, the anti-neuroinflammatory effects of minocycline have established the relationship between the reduction of cytokines/chemokines and microgliosis in AD patient's brain and neuroprotection [10]. Taking into account the critical role played by abnormal post translational modifications on tau protein in the neuropathogenesis of AD, the microtubule-stabilizing agent davunetide was developed, but it failed in Phase II trial in mild to moderate AD patients [11]. On the other hand, methylene blue [12] and its reduced form, leuco-methylthioninium [11], showed high tau aggregation inhibition and affinity for hippocampal cells, being the second generation of methylthioninium dye (TRx0237) in advanced clinical trials due to its improved bioavailability [11].

Finally, anti- $A\beta$ immunotherapy involving anti- $A\beta$ monoclonal antibodies (solanezumab, gantenerumab, and aducanumab) [13] and active vaccines for antibody-induced tau clearance, such as AADvac1, are under investigation for AD treatment [11], but at the moment none of them reached the market [14].

The link between several targets, such as $A\beta$ soluble oligomers in the activation of GSK-3 β , promoting tau-phosphorylation [8,15] and oxidative stress through ROS production [16,17], along with decreased density of nicotinic acetylcholine receptors (nAChR) [18] may entail multitargeting drug development approaches [19]. In fact, the amyloid peptide aggregation induced by the peripheral site (PAS) of AChE [20] led to the synergistic dual binding site AChEI, providing an interesting therapeutic strategy to increase the acetylcholine synapses level (active site-CAS) and modulate $A\beta$ aggregation [21–25]. Thus, based on evidence that both *N*-benzyl piperidine group and indanone moiety of donepezil bind to AChE through CAS and PAS sites, respectively [26], novel indanone-based derivatives containing either *N*-benzylpyridinium [27] or phenyl-piperazine cores [28] were described with moderate to high inhibition of AChE and $A\beta$ -aggregation, anti-oxidant activity and neuroprotection. Besides this multifunctional AChE inhibition, further improvement of anti-oxidant and anti-inflammatory activities, metal-quelating properties and MAO inhibition were achieved for hybrids that just preserve the *N*-benzyl piperidine function of donepezil, but have the indanone core replaced by cinnamoyl [29], feruloyl [30] or 8-hydroxyl-quinolinal groups [31]. Furthermore, tacrine derivatives containing the acridine core are reported as potent inhibitors of AChE, in particular, the known tacrine-donepezil hybrids conserving the indanone moiety (I) [32], or the phthalimide bioisoster (II) [33], and benzylpiperidine/benzylpiperazine units (III, IV) [34,35], related to donepezil structure (Fig. 1).

The high activity of compounds I–IV and the DNA intercalating and highly mutagenic properties of acridine group [36–38] led us to pursue a different hybridization strategy for the synthesis of novel potential dual binding site AChEIs by connecting a simplified and non-toxic quinoline moiety [39], rather than acridine, to indanone core, mimicking both donepezil to interact at peripheral site and tacrine at active site (Fig. 2). In spite of the significant inhibition of hAChE (IC_{50} 73 nM), metal chelation, and self-induced, hAChE-induced and Cu^{2+} -induced $A\beta_{1-42}$ aggregation achieved by

donepezil hybrids containing 2-methyl-pyridine rather than 8-hydroxy-quinoline cores [40], our previous docking studies had shown the promising profile of 4-amino-quinoline nucleolus moiety due to potential interactions with Trp86, His440 and Glu199 residues at the AChE active site [41].

To establish whether this chemical modification should impact on the binding mode of AChE, we have synthetized this new compound, conducted cholinesterase kinetic assays, showing experimentally that this compound acts as dual binding site AChE inhibitor. As a proof of concept, we also used SH-SY5Y cell lines to assess the potential of the hybrid to reverse the neurocytotoxicity induced by $A\beta_{(1-42)}$ peptide (clonogenic assay). Unexpectedly, one of the intermediates compound in the hybrid synthesis has shown a very interesting enzymatic profile. We have found a potent allosteric modulator of AChE able to target cholinergic and non-cholinergic functions by fixing a specific AChE conformation, confirmed by STD-NMR and molecular modeling studies.

2. Results and discussion

2.1. Synthesis

A convergent synthesis strategy was pursued to prepare the intermediate piperidinyl-chloroquinoline (3) by reductive amination between 4-chloro-quinolinyl-2-carbaldehyde (4) and hydroxymethyl-piperidine (5) [42]. Both precursors were obtained straightforwardly by some classical reactions, for instance, ethyl isonipeptate (7) was reduced to the alcohol compound 5 (90% of yields) after treatment with LiAlH₄ in THF [43]. In spite of the 2-methyl-quinoline (6) being commercially available, a modified Friedländer synthesis was explored to obtain the quinoline core, after a cyclization reaction between the cheaper commercial *o*-aminobenzoic acid and acetone in the presence of phosphoryl chloride, to afford the desired compound 6 (40% yield) [44]. The methyl group of 6 was oxidized with SeO₂ and the auxiliary reagent *tert*-butylhydroperoxide to afford the aldehyde 4 in 63% of yields [45]. Thus, the condensation product 3, obtained in 65% yield, submitted to mild oxidation using Dess–Martin reagent gave the aldehyde 8 (36%) [46]. Despite the straight route to obtain the final amino product 15 by replacing the aromatic chlorine atom of intermediate 8 by azide group giving compound 9 (48%) [47] and, then, condensation with indanone 10 to afford product 11 [48], several attempts to reduce the azide group of 11 under hydrogenation conditions were not successful due to formation of complex mixture. For this reason, an alternative strategy was pursued condensing the chlorine aldehyde 8 and indanone 10 in the presence of sodium ethoxide, followed by E1cb elimination reaction to give the E-isomer of α,β -unsaturated chloride, compound 12 (86% yields) [48]. In order to establish the double bound geometry of this enone intermediate, G-BIRD_{R,X}-CPMG-HSQMBC experiments were carried out [49,50] to measure heteronuclear spin-spin coupling constant C–H ($^3J_{CH}$) between olefinic hydrogen and the carbonyl carbon. According to Karplus equation, vicinal coupling constants present a strong correlation with the dihedral angle (θ) enabling correlation of the $^3J_{CH}$ value with E or Z ($\theta = 0^\circ$ or 180° , respectively, for H–C–C–C correlation) stereochemistry of the double bond [51,52]. Thus, in this case, the $^3J_{CH} = 5.9$ Hz was observed in the NMR experiment (compound 12), which corresponds to θ around 0° , confirming the exclusive presence of the expected E isomer, due to the more favorable anti elimination in the E1cb reaction, giving rise to a more stable E-isomer (Support information S-2) [53].

The α,β -unsaturated double bond of compound 12 was reduced after the treatment with NaBH₄ and pyridine, yielding compound 13 (57%) [54]. Finally, starting from either compounds 12 and 13 was possible to replace the chlorine atom to the amine group by

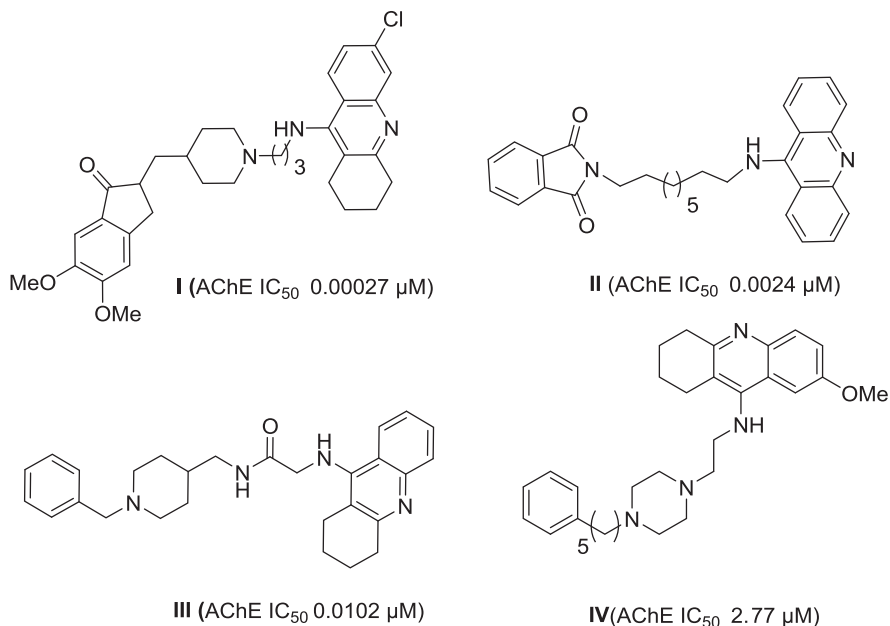


Fig. 1. Tacrine-donepezil hybrids.

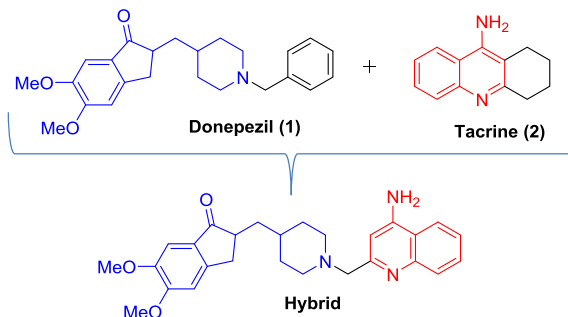


Fig. 2. Hybridization strategy between donepezil (1) and tacrine (2) to the synthesis of novel hybrids dual binding site AChEIs.

cross-coupling Buchwald-Hartwig amination, with 16 and 9% yields for products **14** and **15**, respectively (Scheme 1) [55].

2.2. Cholinesterases inhibition assays

Tacrine-donepezil hybrid and some synthetic intermediates were assayed against human AChE and BuChE by the modified Ellman method [56], using donepezil (**1**) and tacrine (**2**) as references. Compound concentrations corresponding to 50% of enzyme inhibition were calculated based on dose response curves and expressed as IC_{50} (Table 1).

As shown in Table 1, the piperidyl-quinoline precursors, bearing chlorine, compounds **3** and **8**, or azide function, compound **9**, displayed very low inhibitory activity against both *hAChE* and *hBuChE*, requiring additional functionalization. In fact, the condensation of compound **9** with commercial 5,6-dimethoxy-indanone (**10**) afforded the olefin azide **11** with interesting activity against *hAChE*, IC_{50} of 4.88 μM , despite the olefin chlorine intermediate **12**, produced from compound **8**, was not active at the highest tested concentration of 10 μM . In spite of that, the double bond reduction of **12** gave compound **13** with moderate activity against *hBuChE* (IC_{50} 5.99 μM).

Replacement of chlorine atom of olefin **12** by amino group gave

the most active hybrid, olefin **14**, with remarkable activity against *hAChE* in nanomolar range, IC_{50} 0.014 μM . On the other hand, the final reduced product **15** was not active as olefin hybrid **14** (IC_{50} 0.71 μM) when assayed against *hAChE*. In addition, compounds **14** and **15** showed mild *hBuChE* inhibition with IC_{50} 3.69 and 6.54 μM , respectively.

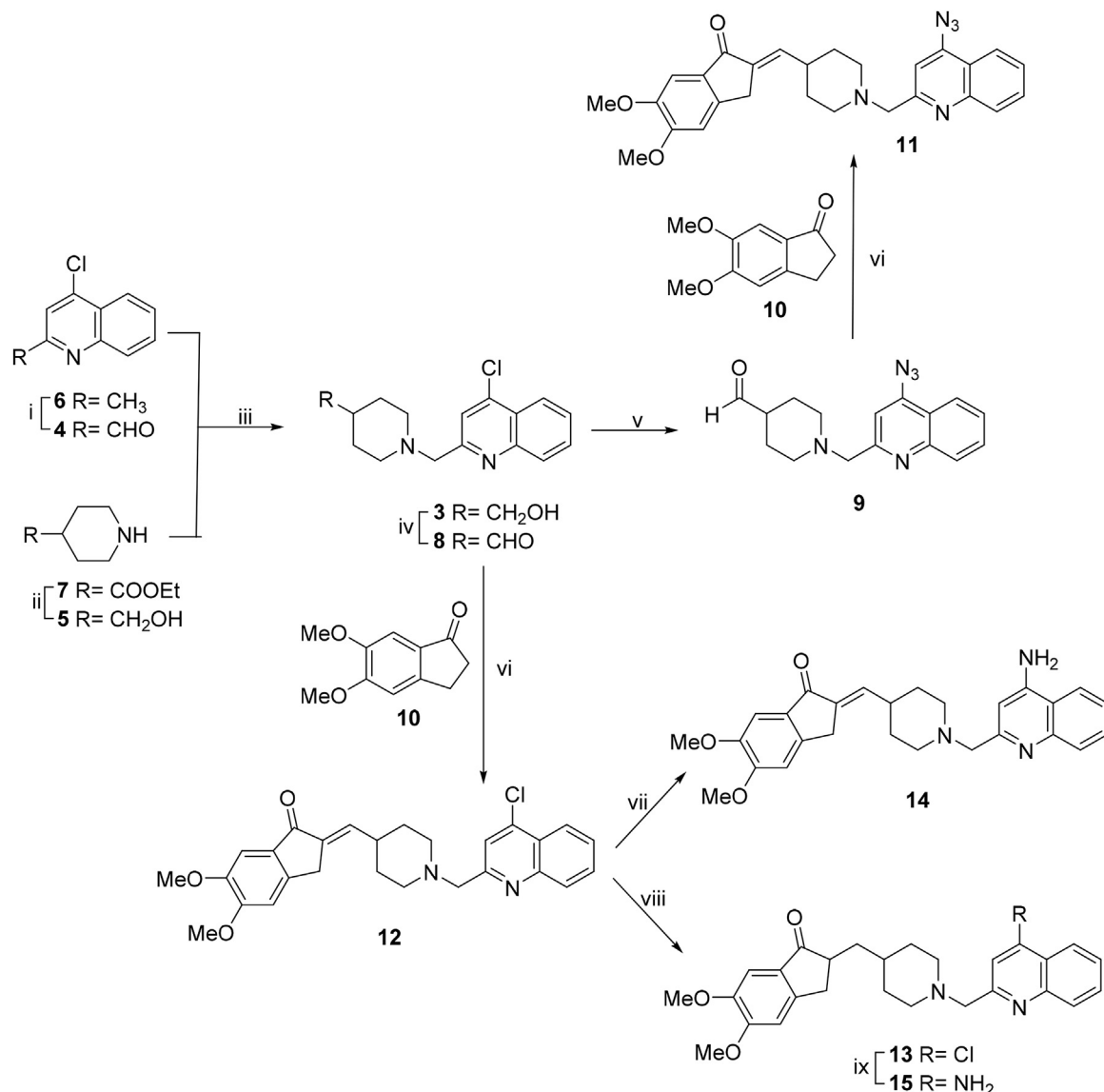
Based on the better activities and chemical structures displayed by compounds **11**, **14** and **15**, we can infer that the scaffolds 5,6-dimethoxy-indanone, quinoline ring and piperidine linker are important for activity. Comparing the olefinic compounds **11** and **14**, having azide or amino groups, respectively, attached to the quinoline ring, it was evident that the amino group had a significant impact on the *hAChE* activity. Besides the effects of amino group, the double bond between the dimethoxy-indanone ring and piperidine linker also affected the enzyme inhibition positively.

Kinetic studies revealed mixed type *hAChE* inhibition for hybrids **11** and **15** (Fig. 3), confirming our initial hypothesis of dual binding site interaction at both peripheral and active sites. Curiously, hybrid **14**, the most active compound of the series, exhibited a clear non-competitive inhibition, as shown in Lineweaver-Burk reciprocal plot below (Fig. 3), which implies an alternative mode of action. Therefore, experimental STD-NMR and extensive molecular modeling studies were explored to better understanding these findings.

2.3. STD competition binding experiments

In order to verify whether two different ligands interact at the same AChE binding site, we followed the STD-NMR method to distinguish competitive from non-competitive binding [57–59]. In principle, STD competition binding experiments lead to the reduction of intensity of the STD signals of the known ligand if a particular ligand targets the same binding site than the known ligand. Alternatively, the same signal intensity of the known ligand is maintained if they bind at a different site [59–61].

Firstly, as control experiments, the STD of the protein at the irradiation point was performed to discard the presence of any contaminant that could interfere in the STD spectrum. In fact, the STD of AChE appears completely clear, with minor NMR



Scheme 1. **i)** SeO_2 , TBHP, dioxane, reflux 1 h. (63%). **ii)** LiAlH_4 , THF, r.t., 24 h. (90%). **iii)** $\text{NaBH}(\text{OAc})_3$, DCE, r.t., 1.5 h. (65%). **iv)** Dess-Martin reagent, CH_2Cl_2 , r.t., 1.3 h. (36%). **v)** NaN_3 , DMF, MW, 70 °C, 150 W, 2.5 h. (48%). **vi)** EtONa , THF, r.t., 24 h. (7%) and (86%) respectively. **vii)** NaBH_4 , Pyridine, 60 °C, 20 min. **viii)** and **ix)** $[\text{Pd}(\text{cinnamyl})\text{Cl}]$ 1 mol%, BippyPhos 4 mol %, NH_4OH (0.5 M), NaOtBu (1.4 equiv), 1,4 dioxane, 110 °C, 3 h. (16%) and (9%) respectively.

Table 1
*h*AChE and *h*BuChE inhibitory activities (μM) of synthesized compounds.

Compounds	IC_{50} <i>h</i> AChE (μM)	IC_{50} <i>h</i> BuChE (μM)
Donepezil (1)	0.0057 ± 0.0005	9.14 ± 0.56
Tacrine (2)	0.23 ± 0.069	0.040 ± 0.002
3	>10	>10
8	>10	>10
9	>10	>10
11	4.88 ± 0.45	>10
12	>10	>10
13	>10	5.99 ± 0.64
14	0.014 ± 0.009	3.69 ± 0.84
15	0.71 ± 0.17	6.54 ± 0.70

spectroscopy signals corresponding to the protein background. In addition, no NMR spectroscopy signals were detected in the STD experiments of merely donepezil (**1**) or **14** at the same irradiation

point (see *Support Information S3-I*).

Afterward, the STD experiment using a AChE/**14** 1:20 M ratio (15.2:304.0 μM) was performed under identical conditions as a control for the experiment (Fig. 4a). Subsequently, additional STD experiments keeping the same 1:20 AChE/**14** M ratio were performed, but in the presence of increasing concentrations of donepezil (**1**). In particular, 80 μM (0.25eq), 304 μM (1.0eq) and 1216 μM (4.0eq) concentrations of **1** were employed (Fig. 4b-d). It was observed that the STD intensities of NMR signals of the hybrid **14** did not significantly decrease in the presence of donepezil (**1**), whereas clear STD signals for the donepezil (**1**) moiety were observed. The alternative experiment was also performed, keeping the AChE/donepezil mixture at a fixed concentration (1:20 M ratio) with adding hybrid **14** at three different concentrations. Identical results to those previously described were observed (see *Support Information S3-II*).

The non-competitive inhibition profile displayed by hybrid **14** based on STD-NMR experiments and kinetics assays led to the

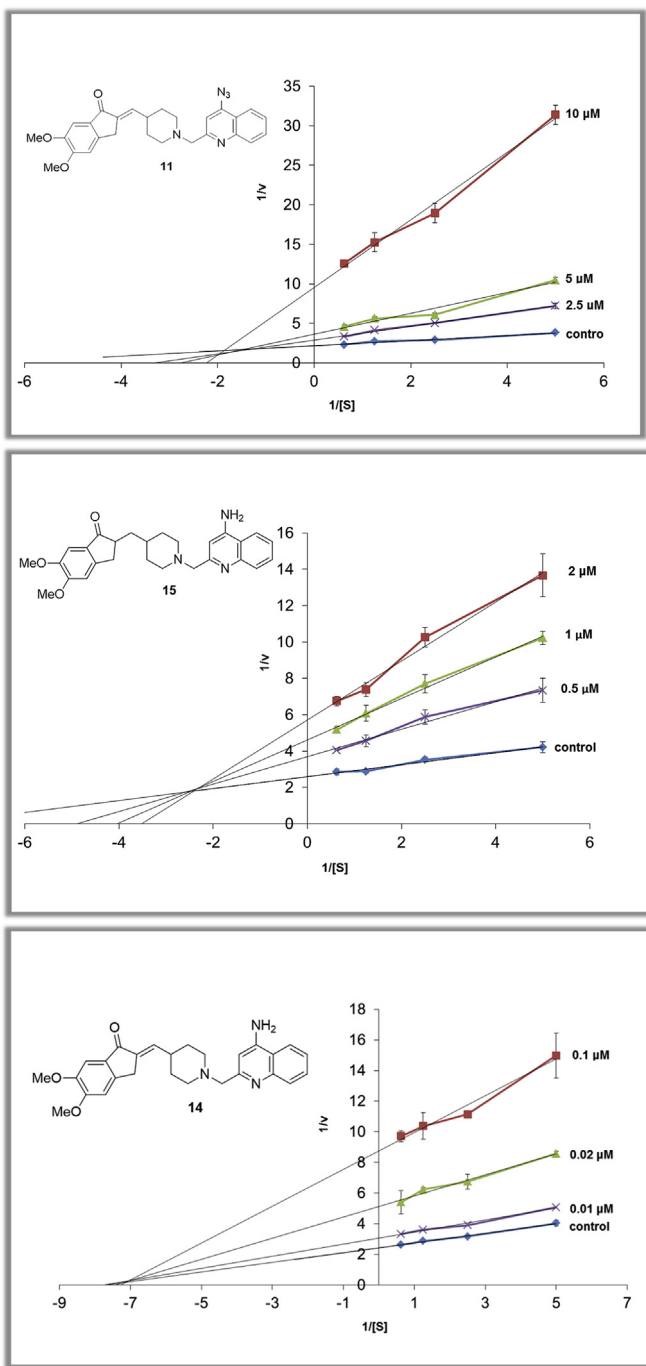


Fig. 3. Lineweaver-Burk plot competitive assays of hybrids **11**, **15** and **14** using hAChE.

investigation of hybrid **11**, which had displayed moderate activity and mixed-type AChE inhibition. In contrast to the observations for **14**, the STD NMR experiments clearly showed a significant decrease (until the disappearance) of the STD intensities of the signals of hybrid **11** (AChE/hybrid **11** mixture) in the presence of donepezil (**1**), as expected for an inhibitor that competes for the same binding site (see [Support Information S3-III](#)). Despite the intrinsic limitations of this method [57,58], the results obtained by STD competition binding experiments strongly suggest that, hybrid **14** may target an allosteric AChE pocket rather than the same binding site of donepezil (**1**).

2.4. Molecular modeling

To evaluate these experimental results, we decided to perform a computational study in order to identify the allosteric binding site of hybrid **14**. The computational studies consisted in a three-steps protocol, firstly, a binding site search using PELE [62] software was applied. This search will allow us to find the most likely cavity where the ligands bind with the best affinities; second, docking studies to find the putative binding mode for this compound in the detected cavity; and finally, molecular dynamics studies were used to refine the protein-ligand complexes, in order to obtain both the more stable protein-ligand complex and to appreciate conformational changes in AChE that could explain the inhibitory activity of compound **14**. Thus, we performed the studies with the potential allosteric modulator **14**, hybrid **12** as negative control and donepezil (**1**) as reference ligand for CAS and PAS interactions at AChE.

2.4.1. Binding site search

A binding site search for donepezil (**1**), hybrid **12** and hybrid **14** using PELE (Protein Energy Landscape Exploration) was performed in order to search the most probable binding cavity for these ligands. Using this script, eight different trajectories for donepezil (**1**), **12** and **14** were computed ([Fig. 5](#)).

The best trajectory found for donepezil (**1**) (Trajectory 5, [Fig. 5](#)) show that the binding mode is very similar to the donepezil (**1**) binding mode present in the crystal structure 4EY7 deposited on the PDB [63] ([Fig. 6](#)), confirming that the ligand is able to enter into the catalytic gorge, which validates our approach. For the inactive, but chemically similar compound **12**, the results of our calculations, show that this compound is not able to bind efficiently to AChE ([Fig. S4-I, S4-II and S4-III](#)).

Regarding the binding energy, a global analysis of all trajectories of the compound **14** shows that in three of the eight trajectories have significantly better binding energy (Trajectories 3, 5 and 7, [Fig. 5](#)). Analyzing these trajectories ([Fig. 7](#)), it is possible to see that in two trajectories the binding site is different from CAS and/or PAS, suggesting an allosteric site, which has been previously recognized in the rosmarinic acid binding to AChE [59]. Furthermore, a recent computational study has been developed by our group in order to describe properly this allosteric binding site, named site B. Some of the key residues of this site are Arg247, Gln291, Arg296, among others [64].

In summary, these preliminary explorations suggest that the hybrid **14** might be an allosteric inhibitor of AChE, due to its binding to the site B ([Fig. 8](#)).

2.4.2. Docking and molecular dynamic studies

Docking and molecular dynamic experiments were developed for compound **14** in order to determine the binding mode for this allosteric inhibitor. Docking calculations were performed using AutoDock [65] with the apo form of AChE (PDB code 4EY4). The results of docking studies for compound **14** showed three important clusters to take into account. The first was related to the most favoured binding energy, the second the most populated and then, the fifth cluster with favorable binding energy and similar population in comparison with the first. The pose of the first cluster has a main ligand-target interaction involving a hydrogen bond between Arg247 and the methoxy group. In addition, the cluster 2 pose has two hydrogen-bonds between Arg247 and Arg296 with the methoxy groups, while the cluster 5 pose has hydrogen bonds between the Asn233 and the carbonyl group and between His405 and methoxy group ([Fig. 9](#)).

The most representative pose of each cluster discussed above

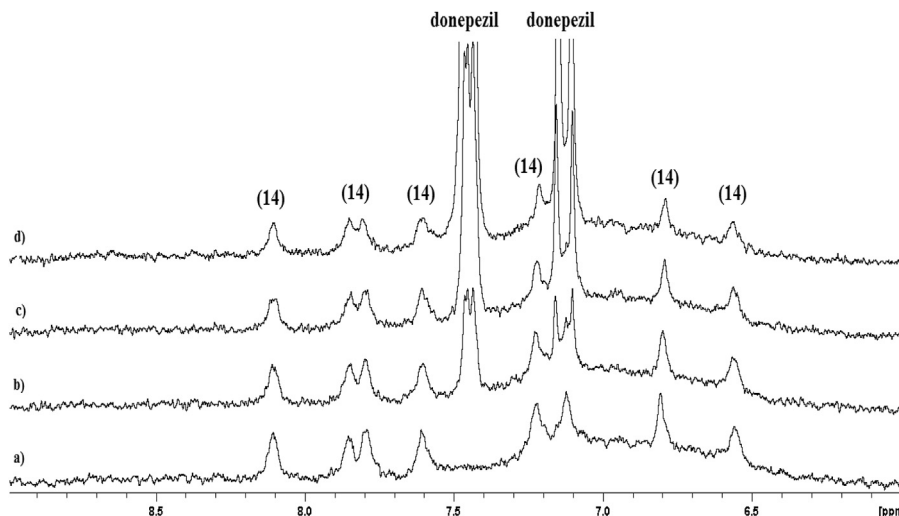


Fig. 4. Expansion of the aromatic region of a) STD spectrum of the system AChE (15.2 μ M)/hybrid **14** (304 μ M); b) STD spectrum of the system AChE (15.2 μ M)/hybrid **14** (304 μ M)/donepezil (80 μ M); c) STD spectrum of the system AChE (15.2 μ M)/hybrid **14** (304 μ M)/donepezil (304 μ M); d) STD spectrum of the system AChE (15.2 μ M)/hybrid **14** (304 μ M)/donepezil (1216 μ M).

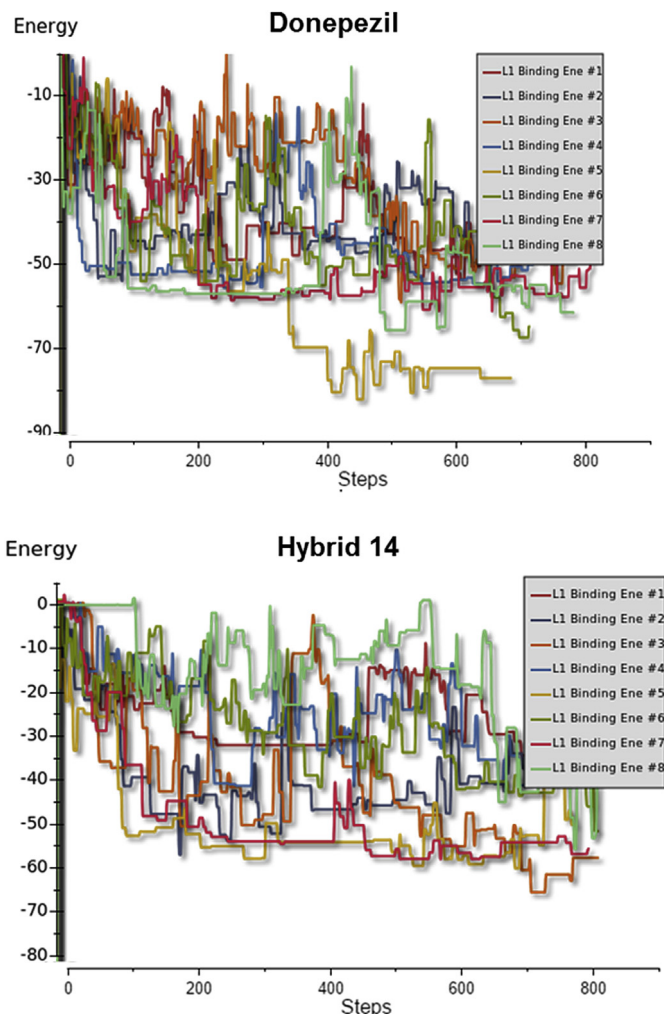


Fig. 5. Binding energy for the eight different trajectories of donepezil-AChE, and hybrid **14**-AChE complexes.

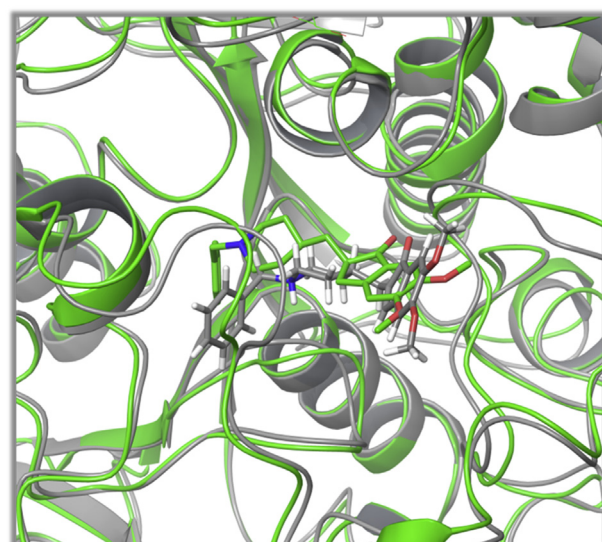


Fig. 6. Superposition of donepezil (1) in complex with AChE in the 4EY7 PDB (green) and donepezil (1) best binding pose obtained with PELE (grey). (For interpretation of the references to colour in this figure legend, the reader is referred to the web version of this article.)

were chosen as the initial point for molecular dynamics studies using AMBER software in order to refine these complexes. Thus, the allosteric mechanism of action could be inferred based on the complex stability and different conformational changes in the AChE target.

Hybrid 14 – Pose Cluster 1. Ligand-Target stability is present during all trajectory, as shown by the root-mean-square deviation (RMSD) variation of the protein backbone (Fig. 10). Along the simulation, the compound maintains a hydrogen bond interaction between the methoxy group of the hybrid **14** and Arg296, a new hydrogen bond with the Gln369 appears during the simulation and maintains over it. This new interaction is important due to the fact that Gln369 is interacting with the Gln291 stabilizing the acyl-loop.

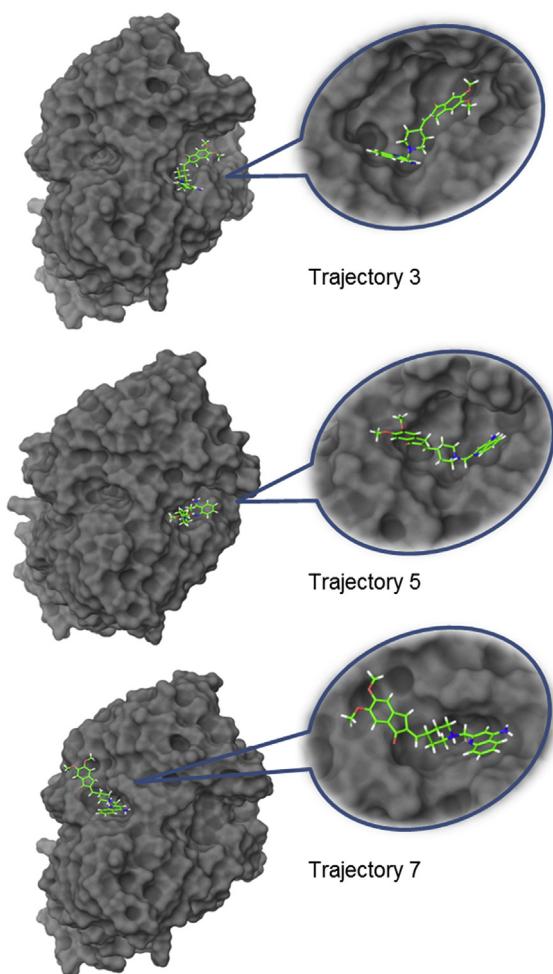


Fig. 7. Best three poses for hybrid **14** in the cavity search. Hybrid **14** in trajectories 3 and 5 is able to recognise the site B pocket, while in trajectory 7 the ligand recognises the entrance of the catalytic gorge, but is not able to enter into this pocket.

When our hybrid **14** ligand interacts with Gln369, the acyl-loop rearranges, moving into the catalytic gorge.

Hybrid 14 - Pose Cluster 2. This ligand pose appears not to be stable during the simulation, since the ligand escapes from the pocket, re-entering in the cavity changing its binding mode. During the simulation, the ligand changes its profile of contacts with the target, showing less stability for this ligand-target complex.

Hybrid 14 - Pose Cluster 5. Cluster 5 shows stable conformation along the simulation, maintaining the interactions with the residues Asn233 and His405.

The trajectories for all simulations were analysed using TRAPP, a computational tool that searches for pocket changes along the molecular dynamics trajectories, showing the different variations and the cavity regions that appear and disappear along the simulation. As hybrid **14** is proposed as an allosteric modulator of AChE, it is possible that its mechanism of action is related to some conformational changes in the catalytic gorge. Thus, TRAPP was used to analyse the possible variations of the catalytic gorge along the simulation.

The catalytic gorge of AChE contains the CAS and PAS regions, and three more different flexible regions that allow the normal function of the enzyme named as side, back and acyl-loop doors [66]. These doors are involved in the exclusion of the degradation products of acetylcholine. Changes in the behaviour of these gates could affect the normal function of the enzyme, modulating its

activity. Another factor that can affect the behaviour of AChE, is the rearrangement in the acyl-loop, that has been proposed in previous studies as a molecular mechanism of the AChE to avoid the reactivation when specific covalent inhibitors bind to the catalytic serine [67]. Hence, taking into account the previous studies about the behaviour of AChE and its mechanism of action, the suggested idea is that flexibility of the catalytic gorge plays a key role in the normal function of the enzyme. Furthermore, the concept of the allosteric modulation has been the object of study and a wide variety of different theories [68] about the existence of allosteric inhibition. One of the proposed theories, defends the possibility that the binding of a ligand in a target cavity can modify the entropy values of the system in such a way that the conformation of the protein is fixed, restricting its movement and thus modifying the target normal behaviour.

Our molecular dynamics studies of the apo form of AChE have revealed that side, back and acyl-loop door appear through the trajectory, due to their flexibility [65] (Fig. 11a). Comparing them with the results for the MD of AChE in complex with hybrid **14**, show that the binding mode found in cluster 1 (Fig. 11b) allows a rearrangement of the acyl-loop, decreasing the volume of the catalytic gorge while this change is not accounted for the other two simulations of hybrid **14** (Fig. S4-IV).

The root mean square fluctuation (RMSF) of the trajectory of hybrid **14** pose (Cluster 1) shows the different regions of AChE that behave in a different way from the apo form (Fig. 12). Side door residues (showed in pink and green) show a restrained movement along the simulation, not allowing the opening of this gate. The restrained movement of the residues that form part of other loops of AChE has been related to (residues 160–168 (yellow), 256–266 (soft pink), 340–346 (cyan) and 368–372 (purple)) target stabilizing effect of our ligand **14**. It is interesting to remark the conformational change in the loop involving residues 302–310 (blue), localized in the bottom of site B. This rearrange is caused by the presence of the ligand in the pocket, promoting this conformational change that increases the pocket surface. In addition, acyl-loop residues (289–295, coloured in orange) in the presence of the ligand show a more rigid behaviour compared to the apo. These findings suggest that hybrid **14** is able to push them into the catalytic gorge, restraining their natural movement.

The binding mode here described for hybrid **14** suggests that both catalytic and peripheral function of AChE may be modulated by the conformational change promoted by the allosteric binding of this compound.

2.5. Cell assays

For the evaluation of cytotoxic effects and hepatotoxicity on SH-SY5Y and HepG2 cell lines, respectively, cells were incubated with seven concentrations of compounds **14** and **15**, based on their AChE IC₅₀, aiming to obtain a dose-dependent effect on cell viability. An inhibition of cell growth was found for both hybrids **14** and **15** tested in SH-SY5Y cells, but only for concentrations higher than 0.056 and 2.84 μM (Fig. 13), respectively. In contrast, no cytotoxicity was observed when donepezil and tacrine was evaluated at the inhibition concentration of AChE IC₅₀ (0.0057 μM and 0.23 μM, respectively).

The results of similar experiments conducted in HepG2 cells showed that compound **14** did not affect cell viability in HepG2 cells; in contrast, the compound **15** was cytotoxic at high concentrations (2.84 and 5.68 μM) (Fig. 14). However, donepezil and tacrine did not show toxicity in the HepG2 cell line within 24 h of treatment, as observed for SH-SY5Y cells. These experiments led us to select three lower concentrations of each compound (0.0035; 0.007; 0.014 μM and 0.088; 0.177; 0.355 μM for **14** and **15**,

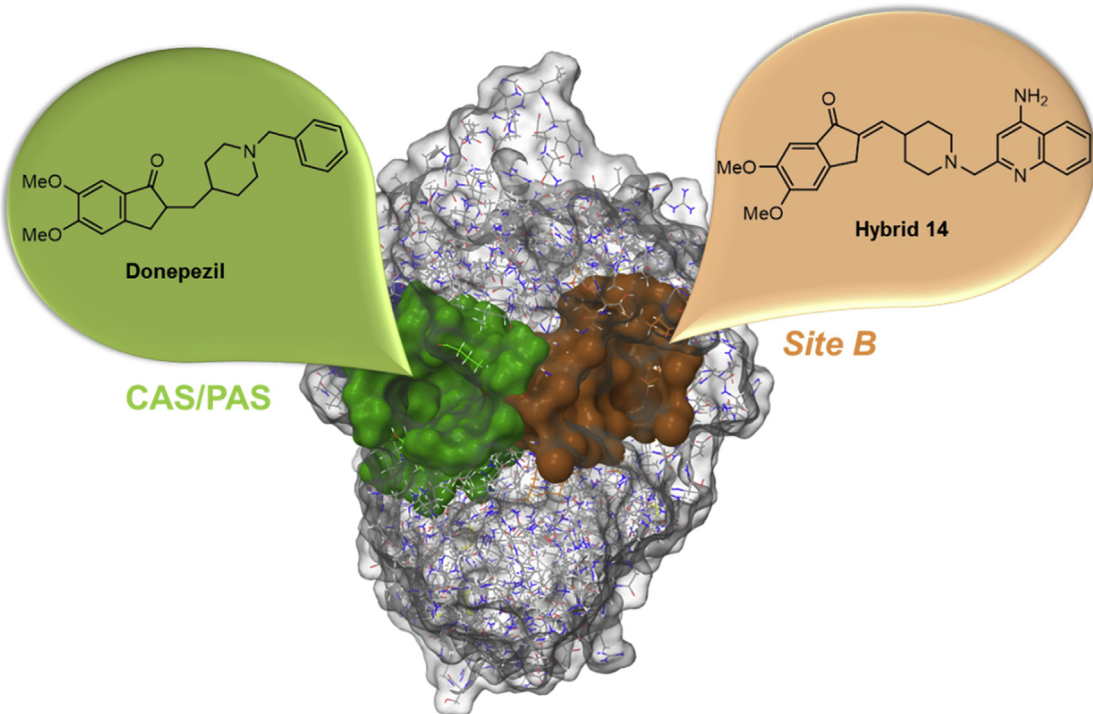


Fig. 8. Surface representation of the detected pockets. CAS/PAS and site B are coloured in green and orange, respectively. (For interpretation of the references to colour in this figure legend, the reader is referred to the web version of this article.)

respectively) to perform other biological assays.

To demonstrate the potential influence of our dual binding site inhibitor **15** in the toxicity promoted by $\text{A}\beta$, a cell based assay was conducted. The allosteric modulator **14** was also assayed to test its biological profile. The effects of these two compounds on human neuroblastoma SH-SY5Y cell lines were assessed due to their neuron-like characteristic comprising the ability of growing and dividing into clumps of cells that can differentiate by extending neurites to the surrounding media. For this purpose, two approaches were used. Firstly, clonogenic assays were pursued to detect the capacity of cells to recover their proliferative properties visualized and quantified as colony formation after damage induction and cell death caused by the treatment with $\text{A}\beta_{(1-42)}$ peptide, which is the most amyloidogenic and neurotoxic isoform of $\text{A}\beta$ peptide found in the brain of AD patients. If our dual binding hypothesis works, we should expect a less aggregation of $\text{A}\beta$ oligomers and so a less toxic effect of this peptide. Subsequently, the influence of our compounds **14** and **15** in inducing the development of neurite elongation and maturation, thus promoting an accurate neuronal interconnection, was evaluated using retinoic acid as positive control to properly induce differentiation of SH-SY5Y cells [69]. It is well recognized that one of the non-cholinergic actions of AChE is neurite promotion [70], which is regulated by a dynamic equilibrium between different interaction sites of AChE [71,72].

Based on clonogenic assays, depicted in Fig. 15, it was evident that the treatment of SH-SY5Y cells with $\text{A}\beta_{(1-42)}$ peptide significantly decreased the survival rate and colony formation when compared to untreated cells. On the other hand, the addition of hybrids **14** and **15** reversed the $\text{A}\beta_{(1-42)}$ peptide-induced inhibition on SH-SY5Y cell proliferation considering the cell recovery rate and cell colony formation compared to cells treated only with the $\text{A}\beta_{(1-42)}$ peptide. The lowest concentrations of both hybrids **14** and **15** (Fig. 15) exerted a better cell recovery at 0.0035 and 0.088 μM , respectively, being the former the most potent regarding the

survival rate slightly above the colony cells formed in the absence of $\text{A}\beta_{(1-42)}$ peptide and tested compounds. The allosteric modulator **14** was the most active derivative in the clonogenic assays with almost complete recovery of survival rates after treatment with $\text{A}\beta_{(1-42)}$ peptide (approx. survival rate 1.1 compared to the control 1.0). Similar experiments performed with drugs **1** and **2** (Fig. 15) at pre-defined concentrations respectively of 0.0057 and 0.23 μM , near AChE IC₅₀, showed only moderate effects (0.6–0.7 in relation to 0.5 cells survival rate treated with $\text{A}\beta_{(1-42)}$ peptide).

Regarding the neural differentiation assay using SH-SY5Y cells (10 days), we found that the compounds **14** and **15** induced morphological changes (Fig. 16), promoting neuronal differentiation and formation of extensive neurites, with decreased cell proliferation, as observed with retinoic acid (RA), known to promote neurodifferentiation [73,74].

To investigate the effect of compounds **14** and **15** on neurite outgrowth in growing SH-SY5Y cells, the percentage of neurite-bearing cells was measured for cells that exhibited extension of at least one neurite presenting a length greater than the diameter of the cell body (Fig. 17). We observed that all compounds tested induced neurite formation when compared to the negative control but in smaller ratio when compared to the RA. As expected, cells treated with the retinoic acid (100%, positive control), showed a marked effect. The percentage of neurite-bearing cells reached $55 \pm 5.0\%$ following treatment with compound **14**, which was significantly higher than the percentage observed for cells treated with the compound **15** ($43 \pm 4.58\%$), donepezil ($33 \pm 5.29\%$) and tacrine ($38 \pm 1.52\%$). All these findings pointed out that the hybrid **14** is the most potent derivative at nanomolar range (0.014 μM) regarding the induction of neurites.

We found that compounds **14** and **15** demonstrated an interesting activity in terms of reversal of toxicity effects caused by $\text{A}\beta_{(1-42)}$ in SH-SY5Y neuroblastoma cells, which were capable of recovering the capacity of cell division and colony formation. In addition,

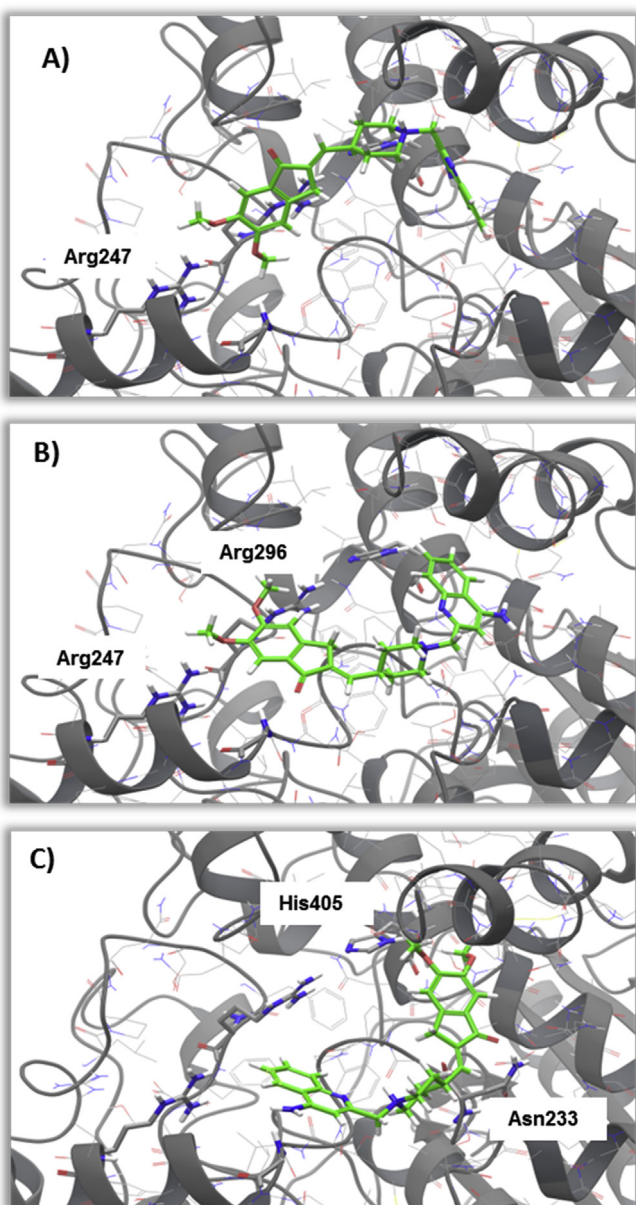


Fig. 9. Best docking solutions for hybrid **14**-AChE. Clusters 1, 2 and 5 are shown in A), B) and C) respectively.

these compounds were able to induce neuritogenesis which is a relevant effect in the promotion of neuronal interconnection, with the possibility to restore synapses failures in the brain. To complement, the AChE inhibition assay also showed promising results, leading to improvements in ACh levels at synapses. Taken together, these interesting results showed that the hybrid **14** represents a valuable hit compound for the development of novel molecules for the therapy of patients with Alzheimer's disease. Moreover, it is a valuable pharmacological tool to explore different non-cholinergic actions of AChE.

3. Conclusion

We have synthesized a dual binding site AChE inhibitor with potent cholinergic activity and neuroprotective profile against A β in a cellular model. Moreover, we have discovered and described an

allosteric modulator of AChE with a low nanomolar *h*AChE inhibitory potency. We have confirmed the allosteric inhibition by kinetic experiments on the enzyme. Furthermore, NMR and molecular modeling studies led to the proposal of new allosteric site on AChE different of the PAS. The promising data from the neuroblastoma cell line, led us to propose hybrid **14** as valuable pharmacological tool for the study of non-cholinergic functions of AChE, and a new important lead for the development of novel disease modifying agents against Alzheimer's disease increasing the cholinergic function, decreasing the A β toxicity and promoting neurite outgrowth.

4. Experimental section

4.1. Cholinesterase inhibition assays

The Ellman's assays were performed in 96 well microplate using human recombinant acetylcholinesterase (*h*AChE) (1000 units/mg protein; lyophilized powder) and human serum butyrylcholinesterase (*h*BChE) (5 units/mg protein, lyophilized powder), purchased from Sigma-Aldrich®. The assay solution is consisted of 0.1 M of phosphate buffer pH 8, 400 μ M 5,5'-dithiobis (2-nitrobenzoic acid) (DTNB, Ellman's reagent), 8 ng.mL $^{-1}$ of AChE or 160 ng.mL $^{-1}$ of BChE, and 800 μ M of acetylthiocholine iodide or 500 μ M of butyrylthiocholine iodide as substrates for AChE and BChE, respectively. Tested compounds (final concentration of 10 μ M) were added to the assay solution and pre-incubated with enzyme over 5 min at 30 °C for subsequent substrate addition. Absorbances were measured at 412 nm over 5 min using spectrophotometer UV/Vis (Multiskan Spectrum, Thermo electron Corporation) and the reaction rates were compared for initial inhibition percentage calculation. The assays were carried out in triplicate and donepezil (**1**) and tacrine (**2**) were used as *h*AChE standard inhibitors. The IC $_{50}$ values were independently determined by performing rate measurements for different concentrations of each tested compound. To investigate the mechanism of action of the tested compounds on cholinesterase, a kinetic analysis was performed. The experiments were carried out using combinations of four substrate concentrations and three inhibitor concentrations with the view to obtain a double reciprocal plot (Lineweaver-Burk), in which each point is mean of three different experiments [56].

4.2. NMR spectroscopy experiments

NMR spectroscopy experiments were recorded on a Bruker Avance 500 MHz spectrometer or a BrukerAvance III spectrometer operating at 600 MHz, with a 5 mm triple-resonance cryogenic probe head. *Electrophorus electricus* acetylcholinesterase (*eel*AChE) enzyme was purchased from Sigma-Aldrich. AChE from *Electrophorus electricus* is a tetramer composed of 4 equal subunits of 70 kDa. Each subunit contains one active site. A solution of AChE from *Electrophorus electricus* was prepared in Tris-d₁₁ buffer (20 mM) at pH 7.4. The concentrations of the compounds were 20–35 fold excess over protein and were prepared from initial stock solutions of each compound in DMSO-d₆. 2D NMR spectroscopy experiments (TOCSY and NOESY) were recorded to acquire additional structural information and to assign donepezil (**1**) and hybrids **11** and **14** ¹H NMR signals using the standard pulse sequences included in the TOPSIN software (Bruker). For the STD experiments, two irradiation frequencies, an off-resonance at δ = 100 ppm (in which no protein signals are present) and an on-resonance at δ = 0 ppm were employed in interleaved fashion and two spectra (off-resonance and on-resonance) were acquired with 1 s irradiation using 50 ms Gaussian-shaped pulses. A total number of 320 scans were acquired and the obtained fids were

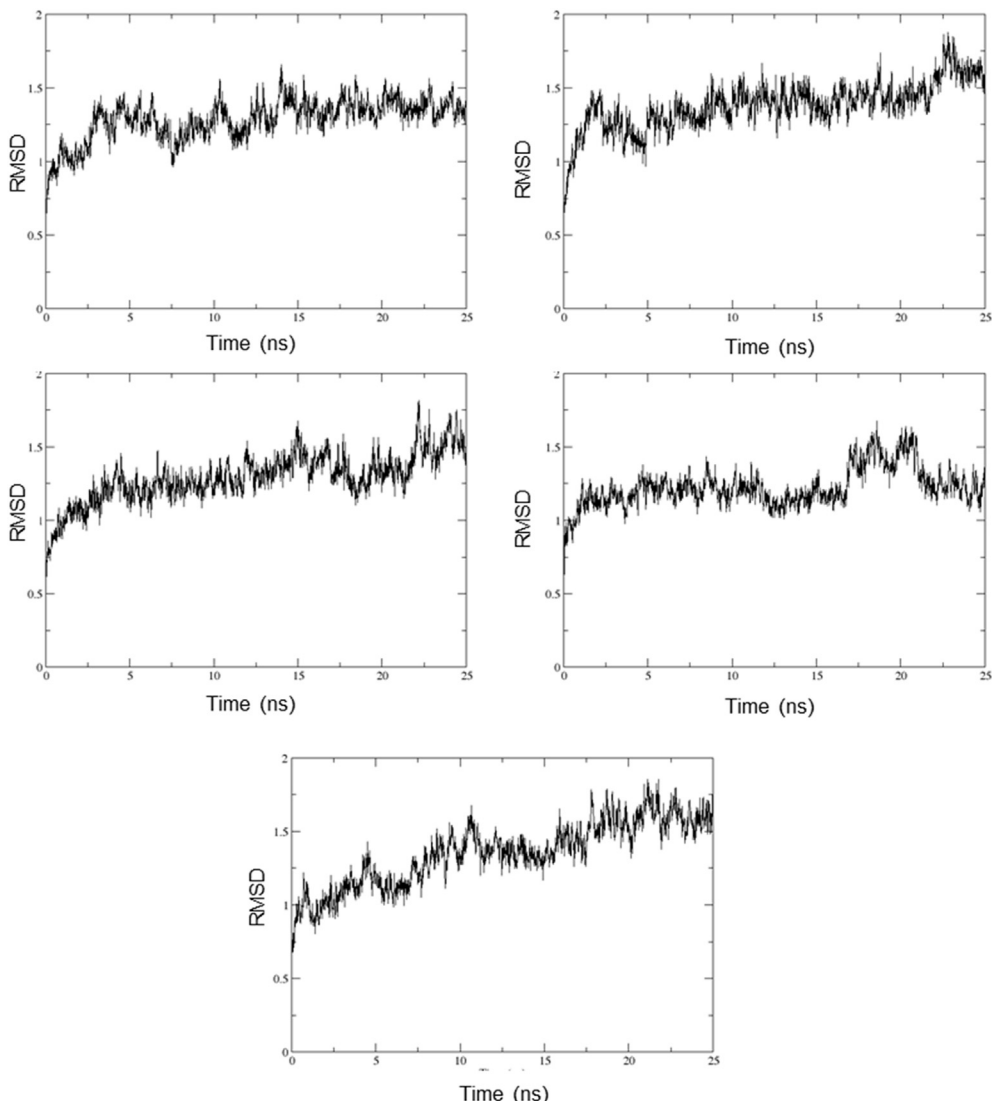


Fig. 10. RMSD of the backbone atoms for the trajectories of AChE without ligand (up-left), hybrid12-AChE (up-right), hybrid14 (cluster1)-AChE (middle-left), hybrid14 (cluster2)-AChE (middle-right), hybrid14 (cluster5)-AChE (down).

multiplied by an exponential line-broadening function of 1 Hz prior to Fourier transformation. STD competition binding experiments were recorded at distinct molar ratios of ligand/protein, however, with a constant protein concentration.

4.3. Molecular modeling

4.3.1. Binding cavity search

Using PELE software [62], the binding cavity search was developed for compound **14**, using donepezil (**1**) as control, in order to validate this protocol. The PDB 4EY4 was used as the target structure. The PDB complex were prepared using Maestro Protein Preparation Wizard [75] tool, adding the hydrogens, ionizing the structure at pH = 7.0 ± 2.0 and removing all ions and waters. PELE combines a Monte Carlo stochastic approach with protein structure prediction algorithms. PELE's protocol is based on a three step algorithm that performs a localized perturbation, by doing a minimization where the alpha carbons are driven to a new position resulting from a small displacement in a low frequency anisotropic normal mode (ANM). The second step is the side chain sampling close to the ligand and finally a minimization is performed to locate the energetic local

minimum. These three steps compose a move that is accepted or rejected based on a Metropolis criterion. Whenever any trajectory is significantly further along than any of the other trajectories, the trailing trajectory is abandoned and restarted from the position of the leading trajectory. This allows an efficient sampling of the configurational space towards one defined objective: the search of the most probable pocket to bind for each ligand.

4.3.2. Docking studies

Docking studies were carried on using AutoDock v4.2 [65]. The 4EY4 structure of hAChE in apo form was selected to develop these studies for hybrid **12** and **14**. Docking studies were centred in the centroid of the best binding energy pose found in PELE cavity search for compound **14**. The grid of 60×60×60 and 0.375 Å of spacing were calculated and the genetic algorithm parameters for the docking studies were 200 genetic algorithm runs, a population size of 150, with a number of evals of 250000. Docking results were analysed through clustering the best 200 poses with 2.0 of RMS.

4.3.3. Molecular dynamics

MD were performed with an Asus 1151 h170 LVX-GTX-980Ti

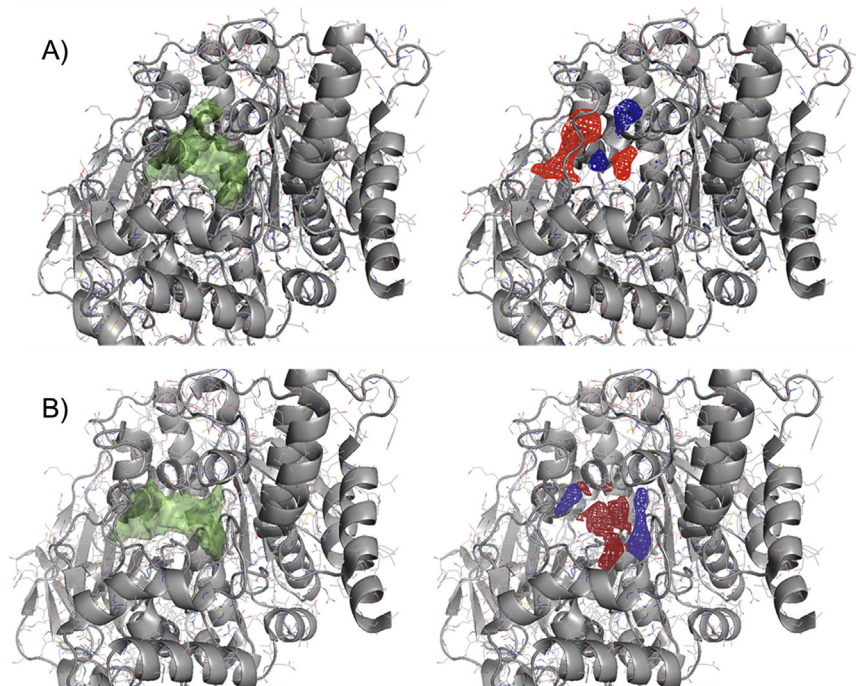


Fig. 11. **A)** Appearing (red) and disappearing (blue) regions along the simulation of AChE apo. The bigger region that appears at the left is related with a movement of the PAS region that opens the side door. The other regions that appear and disappear along the simulation are related with the flexible movement of the residues of the cavity, such as tyrosine, tryptophan or glutamic acid. **B)** Appearing (red) and disappearing (blue) regions along the simulation of AChE in complex with hybrid **14** (Cluster 1). The blue region at the right of the Figure shows that the movement into the cavity of the acyl-loop on occasions reduces the area of the catalytic gorge. (For interpretation of the references to colour in this figure legend, the reader is referred to the web version of this article.)

workstation, with an Intel Core i7-6500 K Processor (12 M Cache, 3.40 GHz) and 16 GB DDR4 2133 MHz RAM. The workstation had Nvidia GeForce GTX 980Ti available for GPU computations. MD using AMBER12 [76] with the ff14SB [77] were developed with two objectives: to refine the docking poses for hybrid **14** and **12**; and to search for a reason of the allosteric mechanism of hybrid **14**. Best three poses for compound **14** and the best pose for compound **12** were selected as starting point for this study. Additionally a MD trajectory for the target without ligand was developed, in order to see the normal behaviour of the AChE and to compare this behaviour with the ligand-target trajectories. RESP charges were calculated using Gaussian09 [78], optimizing the geometry for both compounds using the method HF6-311++(d,p). Systems were solvated using TIP3P model [79] for water molecules, getting into a cubic box, equilibrating the system charge adding Na⁺ ions. Solvated systems were first minimized for 8000 steps with the initial 4500 steps using the steepest descent algorithm. The final 3500 steps used the conjugate gradient energy minimization with constraints applied to the protein residues. This was followed by two minimization stages of 8000 steps, with the last 3500 using the conjugate gradient decreasing the restraints to the system. The system was equilibrated to 300 K and 1 atm, using a 9 steps protocol, applying energetic restraints of 15 kcal mol⁻¹ Å⁻¹ from the initial step and gradually decreasing them until its disappearance. The production trajectories of 25 ns were obtained in isothermal-isobaric ensemble. All bonds involving hydrogen atoms were constrained with the SHAKE algorithm [80]. A cutoff of 10 Å was used for the Lennard-Jones interaction and the short-range electrostatic interactions. Berendsen barostat [81] and Langevin thermostat were used to regulate the system pressure and temperature, respectively. Trajectories of 25 ns were calculated, analysing them using Cpptraj [82] module and VMD [83] for the visual inspection. Xmgrace software [84] was used to obtain the graphics

of RMSD and RMSF of the molecular dynamics simulations. One in every five frames of the trajectories was saved into new trajectories, which were taken to their analysis with TRAPP [85]. The catalytic pocket were analysed using this software, which search for pocket variations along the simulations. Additionally, a PCA analysis for the trajectory was carried out, obtaining the most representatives catalytic pocket models in each trajectory.

4.4. Preparation of beta amyloid peptide A_{β(1-42)}

A_{β(1-42)} peptide was prepared as previously described [86]. The stock solution of A_{β(1-42)} (Sigma-Aldrich, St-Louis, MO, USA) was dissolved at 1 mg/mL in 100% 1,1,1,3,3-hexafluoro-2-propanol (HFIP), sonicated in a water bath for 10 min, aliquoted into micro centrifuge tubes, dried under vacuum and stored at -20 °C. Immediately prior to use, the HFIP-treated A_{β(1-42)} was dissolved in 1 mg/mL dimethylsulfoxide (DMSO). Solution stock of each compound (**14** and **15**) and the standards, donepezil (**1**) (synthesized in our lab as described in the literature [48]) tacrine (**2**) (Sigma-Aldrich) were prepared in DMSO and diluted in HAM F10/DMEM (1:1) medium (Sigma-Aldrich, St. Louis, MO, USA). The final DMSO concentration in the culture medium was less than 0.01 mg/mL.

4.5. Cell line and culture conditions

The SH-SY5Y cell line derived from human neuroblastoma, was purchased from the Rio de Janeiro Cell Bank (Brazil) and the HepG2 cells (human hepatocellular carcinoma) were purchased from the American Type Culture Collection (ATCC), and kindly donated by Dr. Lusania M. G. Antunes (FCFRP-USP). For the experiments, cells were cultured in HAM F10/DMEM (1:1) medium (Sigma-Aldrich, St. Louis, MO, USA) containing 2 mM L-glutamine, 10% Fetal bovine serum (Cultilab, Campinas, SP, Brazil) and 1% penicillin/

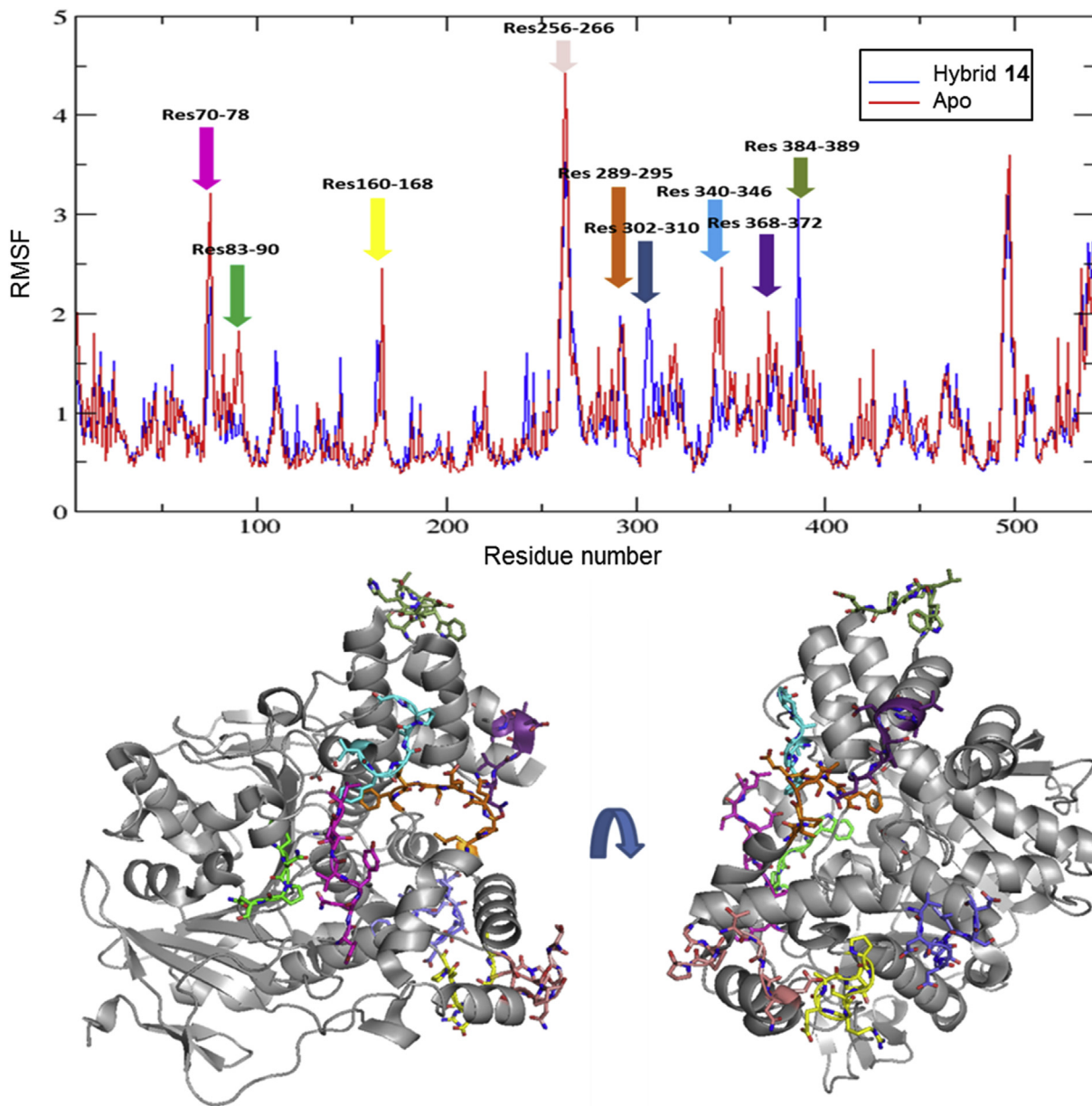


Fig. 12. Root Mean Square Fluctuations per residue along the molecular dynamics simulations of the AChE apo and complexed with hybrid **14**. Below, the structure of hAChE (PDBid 4EY4) with the regions found in the MD simulation is represented. Colour of the residues correlates with the colour of the arrows pointing to the rmsf. (For interpretation of the references to colour in this figure legend, the reader is referred to the web version of this article.)

streptomycin (Sigma-Aldrich, St. Louis, MO, USA) at 37 °C with 5% CO₂ in humidified air. Cells were maintained in proliferation until reaching 80% confluence, when they can be used in the experiments.

4.6. Cell viability

Cell viability assay was performed with the XTT (Cell Proliferation Kit II - XTT, Roche Molecular Biochemicals) colorimetric method. The SH-SY5Y cell line was used to evaluate the cytotoxicity and HepG2 cell line to assess hepatotoxicity of the tested compounds. Cells were plated in 96-well plates (1×10^4 cells/well) and incubated for 24 h at 37 °C in a humidified incubator with 5% CO₂ with different concentrations (based on approximated IC₅₀ values obtained in Ellman's assays) of the compound **14** (0.0035; 0.007;

0.0014; 0.028; 0.056; 0.112 and 0.224 μM); **15** (0.0325; 0.065; 0.13; 0.26; 0.52; 1.04 and 2.08); donepezil (0.0057 μM) and tacrine (0.23 μM); doxorubicin (0.4 μg/mL) was used as positive control. After incubation, cells were washed with PBS and incubated in a fresh medium to allow recovering for 24 h. After this period, the plates were treated with 50 μL of XTT (sodium 30-[1-(phenylaminocarbonyl)-3, 4-tetrazolium]-bis (4-ethoxy-6-nitro) benzene sulfonic acid hydrate). The absorbance was measured at 492 and 690 nm (Epoch Microplate Spectrophotometer, BioTek), according to the manufacturer's protocol. Each treatment was performed in triplicate and data are presented as percentage of the control.

4.7. Clonogenic assay

The procedure to assess clonogenic survival was carried out

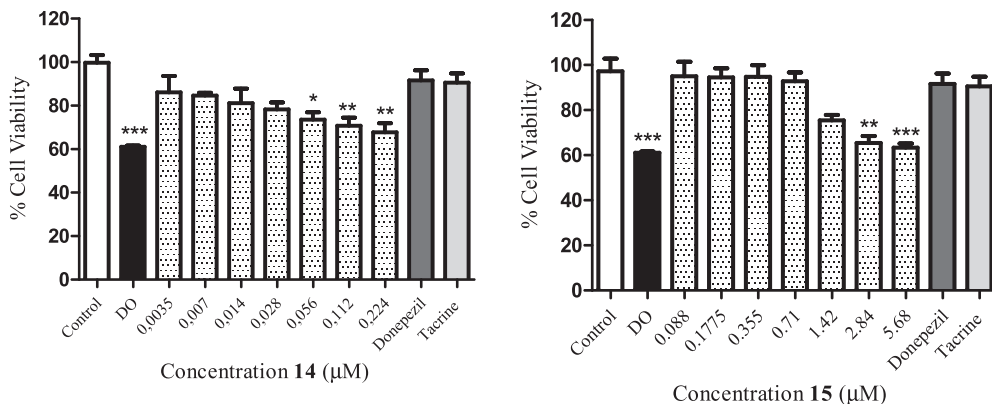


Fig. 13. Cytotoxicity effects of compounds: **14** and **15** evaluated in SH-SY5Y cell line. The cell viability was determined by the XTT assay. Values are expressed as mean \pm SD. * $p < 0.05$, ** $p < 0.01$ and *** $p < 0.001$ indicate statistically significant differences when compared with the Control (untreated cells); DO, doxorubicin (positive control, 0.4 μ g/mL) and donepezil and tacrine (0.0057 μ M and 0.23 μ M, respectively) as standard references.

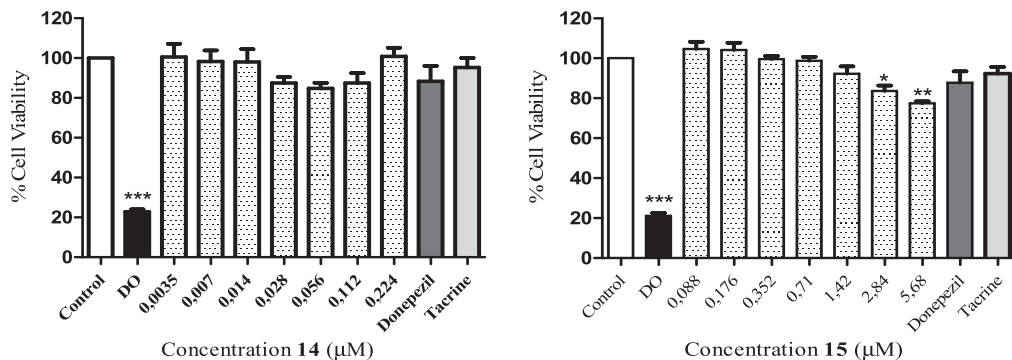


Fig. 14. Hepatotoxicity of **14** and **15** compounds in HepG2 cell line after 24 h. The cell viability was determined by the XTT assay. Values are expressed as mean \pm SD. *** $p < 0.001$; ** $p < 0.01$; * $p < 0.05$ indicate statistically significant differences when compared to the negative Control (untreated cells); DO, doxorubicin (positive control, 0.4 μ g/ml).

according to literature [87] with minor modifications [88]. Cells were grown in 6-well plates at a density of 300 cells/well containing 2 mL of cell culture medium and incubated for 24 h. For each experiment, SH-SY5Y cells were treated with $A\beta_{(1-42)}$ 10 μ M for 24 h. After this period, the medium was removed and replaced with fresh culture medium and the cells were exposed to the three different non-cytotoxic concentrations of each compound **14** (0.0035, 0.007, 0.014 μ M); **15** (0.088, 0.177, 0.355 μ M); donepezil (**1**) (0.0057 μ M) and tacrine (**2**) (0.23 μ M) for 24 h; at the end of the treatments, the medium was removed and cells were rinsed and incubated in a fresh culture medium for 10 days, a period required for the colony formation. After this period, culture medium was discarded and cells were washed with PBS, fixed and stained with Giemsa solution (1: 20 phosphate buffer, pH 7.0) for 10 min. A colony is defined as a cluster of at least 50 clones originated from one cell. Colonies with more than 50 cells were manually counted with the help of an inverted microscope.

4.8. Neuronal differentiation

At first, the SH-SY5Y cells were plated onto 6-well plates (1×10^5 cells per well) in cell medium containing 10% FBS. After 24 h, the medium was removed and replaced by fresh medium containing 1% FBS and drug treatments were performed with 10 μ M of RA (Retinoic acid, positive control), or different IC₅₀ of AChE inhibitors, compound **14** (0.014 μ M), **15** (0.13 μ M), donepezil (**1**) (0.0057 μ M) or tacrine (**2**) (0.23 μ M). The culture medium was removed every three days (4, 7 and 10 days) to replace drug

treatments; following 10 days of treatment, cells were collected and prepared for the experiments. The quantification of neurite proliferation was performed for cells that exhibited extension of at least one neurite presenting a length greater than the diameter of the cell body, according to literature [89], with minor modifications. The images were captured using an inverted-phase microscope (Nikon, Tokyo, Japan), at a magnification of 40 \times , and 100 cells taken from random fields were counted for each treatment in order to identify the neurite-bearing cells.

4.9. Statistical analysis

Data obtained from three independent experiments with respective duplicates are expressed as mean \pm standard deviation (S.D.). Statistical analysis was performed by an overall one-way analysis of variance (ANOVA) and Bonferroni post hoc test, using GraphPad Prism Version 5.01 for Windows (GraphPad Software Inc. USA). A p-value lower than 0.05 denoted a statistically significant difference.

4.10. Chemistry

300 MHz ¹H/75.5 MHz; 400 MHz ¹H/100.6 MHz ¹³C NMR; 500 MHz ¹H/125.8 MHz and 600 MHz ¹H/150.9 MHz ¹³C NMR spectra were recorded in CDCl₃ or CD₃OD on Bruker Advance DPX-300, DRX-400, DRX-500 and Bruker Avance III HD 600 Triple Inverse TCI Cryo-probehead spectrometers, the chemical shifts are reported in ppm (δ scale) relative to internal tetramethylsilane, and coupling constants

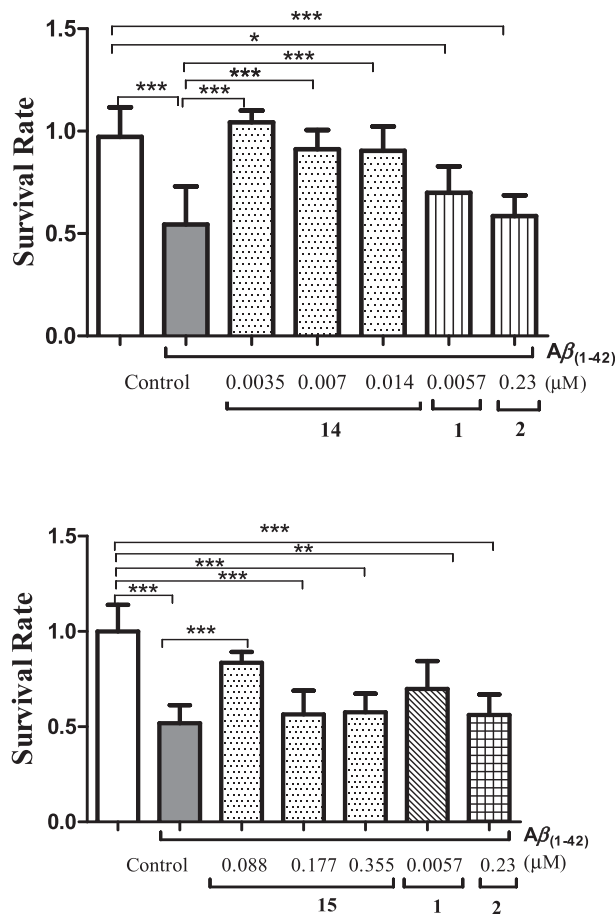


Fig. 15. Survival cell rate of SH-SY5Y cells after exposure to $A\beta_{(1-42)}$ and treatment with: **14** and **15**. Data are means \pm SD calculated from three independent experiments, each performed in duplicate. * $p < 0.05$; ** $p < 0.01$ and *** $p < 0.001$ indicate statistically significant differences. Control (untreated cells); Positive control: cell treated with $A\beta_{(1-42)}$.

are reported in hertz (Hz). The assignment of chemical shifts was based on standard NMR experiments (^1H , ^{13}C -DEPT, ^1H -COSY, HSQC, HMBC). The microwave-assisted reaction was performed in sealed tubes on a CEM Discover® Microwave System. Melting points were measured on a Thermo Fisher apparatus and are uncorrected. Column chromatography was performed on flash silica gel 60 (40–60 mesh, SDS). Thin-layer chromatography was performed with aluminum-backed sheets with silica gel 60 F254 (Merck), and spots were visualized with UV light. HPLC purification of compound **15** was performed on a Shimadzu SCL-10AVP with diode array detector (DAD), analytical column C18 CLC-ODS (M) (150 mm \times 4.6 mm) and semipreparative column Phenomenex Luna C18 (250 \times 10 mm) were used as well. High resolution Mass spectroscopy was performed in a Bruker Daltonics ULTRO-Q-TOF.

4.10.1. 4-Piperidinylmethanol-1-[(4-chloroquinoline-2-yl)methyl] (3)

To a mixture of 4-hydroxy-methylpiperidine (**5**) (0.160 g; 1.39 mmol), dichloroethane (1.10 mL) and molecular sieves 4 Å (0.101 g) under nitrogen protection was added 4-chloroquinoline-2-carbaldehyde (**4**) (0.202 g; 1.05 mmol), the mixture was stirred at room temperature for 1 h. After, the $\text{NaBH}(\text{OAc})_3$ (0.328 g; 1.5 mmol) was added and stirred for more 1.5 h. To work up, was added 3.0 mL de NaHCO_3 , stirred for 10 min, filtered through sintered glass filter celite pad, washed with dichloromethane and portioned

with NaCl sat. Following solvent removal, the crude material was purified by flash chromatography with dichloromethane:ethyl acetate gradient to afford compound **3** 65% (0.197 g) yield. Mp 107–108 °C; ^1H NMR (400 MHz, CDCl_3) δ : 8.21 (1H, dd, J = 8.4; 1.0 Hz, H-9), 8.08 (1H, d, J = 8.4 Hz, H-6), 7.78 (1H, s, H-3), 7.75 (1H, ddd, J = 8.4; 6.9; 1.4 Hz, H-8), 7.61 (1H, ddd, J = 8.2; 6.9; 1.2 Hz, H-7), 3.79 (2H, s, H-11), 3.53 (2H, d, J = 6.4 Hz, H-17), 2.94 (2H, d, J = 11.6 Hz; H-12 eq; H-16 eq), 2.16 (2H, td, J = 11.7; 2.4 Hz, H-12ax; H-16 ax), 1.74 (2H, d, J = 12.5 Hz, H-15eq; H-13eq), 1.61–1.49 (1H, m, H-14), 1.36 (2H, ddd, J = 12.2; 3.8 Hz, H-15ax; H-13ax). ^{13}C NMR (400 MHz, CDCl_3) δ : 28.8 (C15, C13), 38.4 (C14), 53.8 (C16, C12), 65.2 (C11), 67.9 (C17), 121.0 (C3), 125.6 (C4), 124.0 (C9), 127.1 (C7), 129.3 (C8), 130.3 (C6), 143.0 (C5), 148.4 (C10), 160.3 (C2). HRMS (ESI): m/z [M+H]⁺ calcd for $\text{C}_{16}\text{H}_{19}\text{ClN}_2\text{O}$ 291.1259, found m/z [M+H]⁺ 291.1288.

4.10.2. 4-Chloroquinoline-2-carbaldehyde (**4**)

To a solution of SeO_2 (1.44 g; 13.0 mmol) in 11.2 mL of dioxane, was dropwise added 540 μ L of *tert*-butylhydroperoxide (70% aqueous solution). The reaction mixture was stirred at room temperature for 30 min. Then, was added the compound 4-chloro-2-methylquinoline (**6**) (1.0 g; 5.65 mmol) and refluxed for 1 h. After, the suspension was filtered through sintered glass filter celite pad, washed with dichloromethane, and portioned with NaCl sat. Then, the solvent was removed under reduced pressure and the crude product was purified by automated flash chromatography [hexane:ethyl acetate, 8:2] to afford the desired compound **4**. 63% (0.6767 g) yield; ^1H NMR (400 MHz, CDCl_3) δ : 10.18 (1H, s, H-11), 8.31 (1H, dd, J = 8.4; 1.4, H-9), 8.27 (1H, dd, J = 8.3; 0.8 Hz, H-6), 8.09 (1H, s, H-3), 7.89 (1H, ddd, J = 8.4; 6.9; 1.4, H-8), 7.80 (1H, ddd, J = 8.3; 7.0; 1.3 Hz, H-7). ^{13}C NMR (400 MHz, CDCl_3) δ : 117.6 (C3), 124.4 (C9), 128.0 (C4), 130.2 (C7), 130.8 (C8), 131.3 (C6), 144.2 (C5), 148.6 (C10), 152.3 (C2), 192.6 (C11). HRMS (ESI): m/z [M+H]⁺ calcd for $\text{C}_{10}\text{H}_6\text{ClNO}$ 192.0211, found m/z [M+H]⁺ 192.0211.

4.10.3. 4-Hydroxy-methylpiperidine (**5**)

The procedure was followed as described in literature [43]. 90% yield. ^1H NMR (400 MHz, CDCl_3) δ : 3.47 (2H, d, J = 6.4 Hz, H-7), 3.11 (2H, dt, J = 11.9, 3.0 Hz, H-2eq, H-6eq), 2.61 (2H, td, J = 12.3, 2.6 Hz, H-2ax, H-6ax), 2.24 (br s, 2H, NH/OH), 1.74 (2H, d, J = 13.6 Hz, H-5eq, H-3 eq), 1.68–1.56 (1H, m, H-4), 1.16 (2H, ddd, J = 12.1, 4.1 Hz, H-5ax, H-3ax). ^{13}C NMR (400 MHz, CDCl_3) δ : 29.7 (C3 and C5); 38.9 (C4); 46.2 (C2 and C6); 68.0 (C7). HRMS (ESI): m/z [M+H]⁺ calcd for $\text{C}_6\text{H}_{13}\text{NO}$ 116.1070, found m/z [M+H]⁺ 116.1065.

4.10.4. 4-Chloro-2-methylquinoline (**6**)

The procedure was followed as described in literature [44]. 40% yield; ^1H NMR (400 MHz, CDCl_3) δ 8.10 (1H, dd, J = 8.4; 1.0 Hz, H-9), 7.96 (1H, d, J = 8.4 Hz, H-6), 7.66 (1H, ddd, J = 8.4; 7.0; 1.4 Hz, H-8), 7.51 (1H, ddd, 8.4; 7.0; 1.0, H-7), 7.33 (1H, s, H-3), 2.65 (3H, s, H-11). ^{13}C NMR (400 MHz, CDCl_3) δ : 25.2 (C11); 122.0 (C3); 123.9 (C9); 124.7 (C4); 126.7 (C7); 128.9 (C8); 130.4 (C6); 142.6 (C5); 148.7 (C10); 158.9 (C2). HRMS (ESI): m/z [M+H]⁺ calcd for $\text{C}_{10}\text{H}_8\text{ClN}$ 178.0418, found 178.0418.

4.10.5. 4-Piperidinylaldehyde-1-[(4-chloroquinolin-2-yl) methyl] (**8**)

To a *Dess-Martin* periodinane solution (0.1095 g; 0.2584 mmol) in anhydrous dichloromethane (1.0 mL), under nitrogen atmosphere was dropwise added a solution of the alcohol 4-piperidinylmethanol-1-[(4-chloroquinolin-2-yl)methyl] (**3**) (0.0505 g; 0.1723 mmol) in anhydrous dichloromethane (0.9 mL) and stirred for 1.3 h. To work up, was added 5.5 mL ethyl ether, 3.3 mL of a saturated solution of NaHCO_3 and 12 mL of a solution of $\text{Na}_2\text{S}_2\text{O}_3$ (1.57 Mol/L) and then stirred for 20 min. After, the aqueous phase was extracted with ethyl ether (3 \times de 10 mL), and the ether

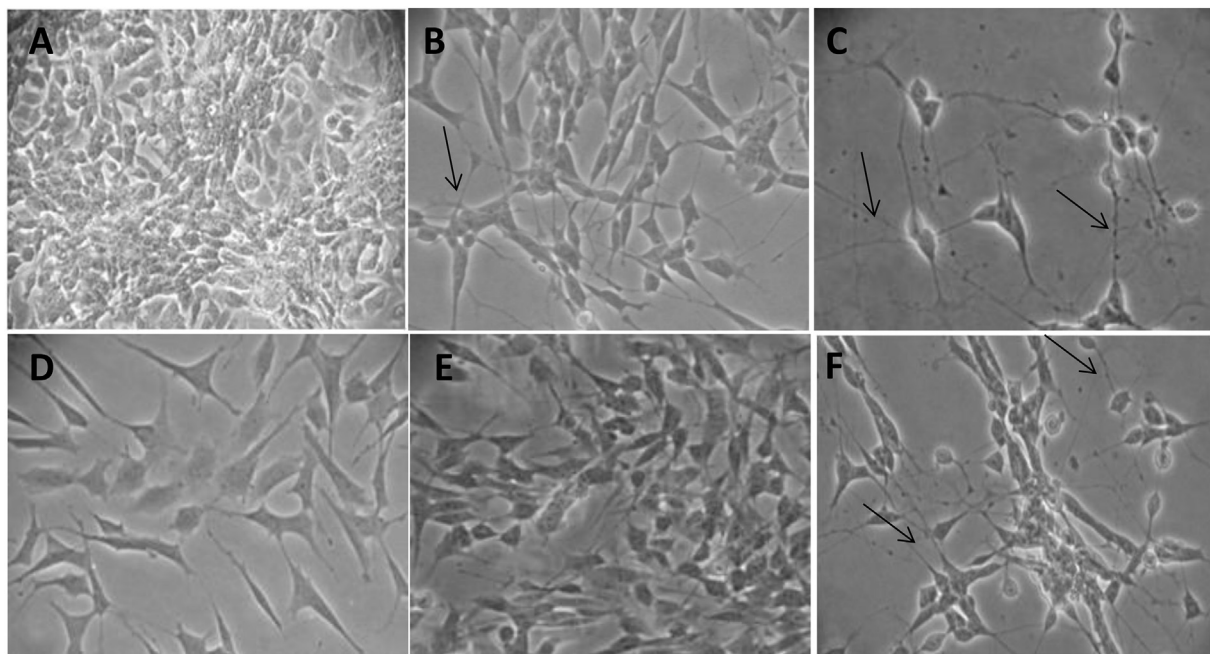


Fig. 16. Morphology of differentiated SH-SY5Y cells continuously treated with compounds **14–15** for 10 days. Panel (A): Control untreated cells; panel (B) Cells treated with compound **14**; panel (C) compound **15**; panel D: Cells exposed to donepezil (**1**); panel E: Cells exposed to tacrine (**2**) and panel F: Cells exposed to retinoic acid (positive control). Arrows indicate neurite formation in cells at late differentiation stage.

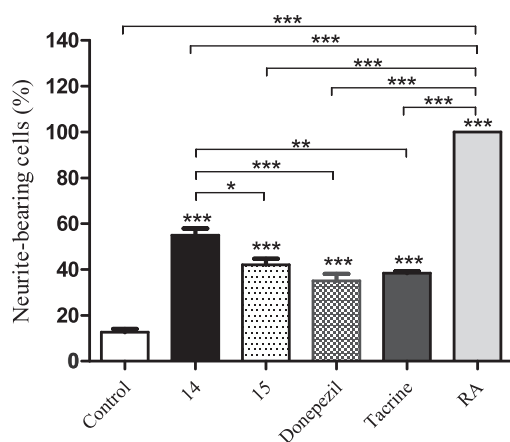


Fig. 17. Effects of the compounds **14** and **15** in the formation of neurites after 10 days of differentiation. Percentage of neurite-bearing cells in SH-SY5Y cell line was measured for cells that exhibited extension of at least one neurite presenting a length greater than the diameter of the cell body. RA: retinoic acid, 10 μ M (positive control); compound **14** (0.014 μ M); **15** (0.13 μ M); donepezil (**1**) (0.0057 μ M); tacrine (**2**) (0.23 μ M). Values are expressed as mean \pm SD. *** p < 0.001; * p < 0.05 indicate statistically significant differences.

phase was washed with saturated solution of NaHCO_3 (3×10 mL). The organic phase was concentrated under reduced pressure, and the crude material was purified by flash chromatography with dichloromethane:ethyl acetate gradient. Yields 36% (0.017 g); ^1H NMR (400 MHz, CDCl_3) δ : 9.60 (1H, d, J = 1.0, H-17), 8.14 (1H, dd, J = 8.4; 0.9 Hz, H-9), 8.00 (1H, dd, J = 8.4; 0.4 Hz, H-6), 7.69 (1H, s, H-3), 7.68 (1H, ddd, J = 8.4; 7.0; 1.4 Hz, H-8), 7.55 (1H, ddd, J = 8.2; 7.0; 1.2 Hz, H-7), 3.75 (2H, s, H-11), 2.83 (2H, dt, J = 11.1; 3.6 Hz, H-12 eq; H-16 eq), 2.30–2.17 (3H, m, H-14; H-12ax; H-16 ax), 1.84–1.91 (2H, m, H-15eq; H-13eq), 1.69 (2H, ddd, J = 10.7, 3.7 Hz, H-15ax; H-13ax). ^{13}C NMR (400 MHz, CDCl_3) δ : 25.3 (C13 e C15),

47.6 (C14), 52.8 (C12 e C16), 64.7 (C11), 121.0 (C3), 124.0 (C9), 125.7 (C4), 127.3 (C7), 129.3 (C6), 130.4 (C8), 143.2 (C5), 148.4 (C10), 159.4 (C2), 203.7 (C17). HRMS (ESI): m/z [M + H $^+$] calcd for $\text{C}_{16}\text{H}_{17}\text{ClN}_2\text{O}$ 289.1102, found m/z [M + H $^+$] 289.1117; m/z [(M + H $^+$) $+ \text{H}_2\text{O}$] 307.1214.

4.10.6. 4-Piperidinylaldehyde-1-[(4-azidoquinolin-2-yl)methyl] (**9**)

In a sealed and dried microwave tube, were added 0.100 g (0.347 mmol) of aldehyde **8**, 1.00 mL of anhydrous DMF and (0.132 g; 2.03 mmol) of sodium azide and stirred under argon protection for 10 min. After, the mixture was heated by microwave irradiation (2.5 h; 70 °C; 150 W). The crude material was purified by automated flash chromatography (Biotage®), isocratic ethyl acetate, yield 48% (0.005 g). IR: 2117; 1719 cm^{-1} . ^1H NMR (300 MHz, CDCl_3) δ : 9.68 (1H, d, J = 0.9 Hz, H-17), 8.06–8.00 (2H, m, H-9, H-6), 7.72 (1H, ddd, J = 8.4, 6.9, 1.4 Hz, H-8), 7.51 (1H, ddd, J = 8.1, 6.9, 1.1 Hz, H-7), 7.43 (1H, s, H-3), 3.80 (2H, s, H-11), 2.90 (2H, dt, J = 11.5, 3.7, H-12eq, H-16eq), 2.29 (3H, ddd, J = 14.0, 8.2, 2.7, H-12ax, H-16ax, H-14), 1.96 (2H, m, H-15eq, H-13eq), 1.83–1.65 (2H, m, H-13ax e H-15ax). ^{13}C NMR (75 MHz, CDCl_3) δ : 203.7 (C17), 160.1 (C2), 148.6 (C10), 146.6 (C5), 130.4 (C8), 128.8 (C6), 126.1 (C7), 122.2 (C9), 120.9 (C4), 108.1 (C3), 65.3 (C11), 52.9 (C12 and C16), 47.8 (C14), 25.5 (C13 and C15). HRMS (ESI): m/z [M + H $^+$] calc 296.1506, found m/z [M + H $^+$ + MeOH] 328.1768; [M + H $^+$ - N₂] 268.1282.

4.10.7. (E)2-((1-((4-Azidoquinolin-2-yl)methyl)piperidin-4-yl)methylene)-5,6-dimethoxy-2,3-dihydro-1*H*-inden-1-one (**11**)

In a dried round three necks bottom flask, under argon atmosphere, were added (0.0206 g; 0.107 mmol) of commercial 5,6 dimethoxy-1-indanone (**10**), powder molecular sieves 4 Å (0.030 g) (previously dried in muffle oven 300 °C for 6 h), anhydrous THF (1.5 mL) and sodium ethoxide (0.0102 g; 0.146 mmol) were stirred for 20 min to form the enolate. After, was dropwise added the aldehyde **9** (0.0371 g; 0.128 mmol) solubilized in 1.5 mL of THF, the resulting mixture was stirred for 24 h, at room temperature. After the reaction completed, the crude mixture was purified by

automated flash chromatography (Biotage®), hexane: acetyl acetate gradient, yield 7% (0.003 g).

IR: 1693; 1647; 2117 cm⁻¹. ¹H NMR (400 MHz, CDCl₃) δ 8.07–7.99 (2H, m, H-9, H-6), 7.72 (1H, ddd, J = 8.5, 6.9, 1.4 Hz, H-8), 7.51 (1H, ddd, J = 8.7, 4.9, 1.3 Hz, H-7), 7.48 (1H, s, H-3), 7.30 (1H, s, H-23), 6.91 (1H, s, H-26), 6.69 (1H, dt, J = 9.7, 1.7 Hz, H-17), 3.93 (3H, s, H-28), 3.98 (3H, s, H-27), 3.83 (2H, s, H-11), 3.62 (2H, d, J = 1.5 Hz, H-19), 2.99 (2H, d, J = 11.5 Hz, H-12eq, H-16eq), 2.33–2.45 (2H, m, H-13eq, H-14), 2.26 (2H, dt, J = 11.4, 3.4 Hz, 12-ax, 16-ax), 1.79–1.65 (3H, m, 13-ax, 15-ax, 15-eq). ¹³C NMR (101 MHz, CDCl₃) δ 192.6 (C22), 160.3 (C2), 155.4 (C24), 149.5 (C25), 148.6 (C10), 146.6 (C5), 144.6 (C20), 139.7 (C17), 135.8 (C18), 130.4 (C8, C21), 128.7 (C6), 126.1 (C7), 122.2 (C4, C9), 108.3 (C3), 107.3 (C26), 105.1 (C23), 65.6 (C11), 56.3 (C28), 56.2 (C27), 53.6 (C12 and C16), 37.1 (C14), 31.3 (C19), 29.7 (C13), 29.5 (C15). HRMS (ESI): C₂₇H₂₇N₅O₃ m/z [M + H⁺] calc 470.2187 found m/z [M + H⁺] 470.2186.

4.10.8. (E) 2-((1-((4-Chloroquinolin-2-yl)methyl)piperidin-4-yl)methylene)-5,6-dimethoxy-2,3-dihydro-1H-inden-1-one (12)

To a mixture of 5,6-dimethoxy-1-indanone (**10**) (0.0445 g; 0.2316 mmol) in anhydrous THF (1.5 mL) under argon protection was added EtONa 95% (0.0266 g; 0.3910 mmol), and stirred at room temperature for 30 min. After, was dropwise added a solution of aldehyde **8** (0.080 g; 0.2770 mmol) in THF (1.5 mL), and stirred for 20 h. The mixture was partitioned with dichloromethane and NaCl sat, the organic phase was concentrated under reduced pressure and the crude material was purified by flash chromatography with dichloromethane:ethyl acetate gradient. Yields: 86% (0.092 g); mp: 189–191 °C. IR: 1688; 1656 cm⁻¹. ¹H NMR (400 MHz, CDCl₃) δ: 8.22 (1H, d, J = 9.3 Hz, H-9), 8.08 (1H, d, J = 8.4 Hz, H-6), 7.80 (1H, s, H-3), 7.75 (1H, ddd, J = 8.4; 7.0; 1.4 Hz, H-8), 7.62 (1H, ddd, J = 8.2; 7.0; 1.0 Hz), 7.30 (1H, s, H-23), 6.91 (1H, s, H-26), 6.69 (1H, dd, J = 8.0; 1.7, H-17), 3.97 (3H, s, H-27), 3.93 (3H, s, H-28), 3.83 (2H, s, H-11), 3.61 (2H, d, J = 1.3 Hz, H-19), 2.94–3.02 (2H, m, H-16eq, H-12eq), 2.32–2.42 (2H, m, H-13eq, H-14), 2.25 (2H, td, J = 11.2; 3.4 Hz, H-12ax, H-16ax), 1.67–1.78 (3H, m, H-13ax, H-15ax, H-15eq). ¹³C NMR (400 MHz, CDCl₃) δ: 29.5 (C19), 31.2 (C13, C15), 37.1 (C14), 53.5 (C12, C16), 56.2 (C27), 56.3 (C28), 65.2 (C11), 105.0 (C23), 107.2 (C26), 121.0 (C3), 124.0 (C9), 125.6 (C4), 127.1 (C7), 129.3 (C6), 130.3 (C8), 131.8 (C21), 135.8 (C18), 139.6 (C17), 143.1 (C5), 144.5 (C20), 148.4 (C10), 149.5 (C25), 155.3 (C24), 160.0 (C2), 192.6 (C22). HRMS (ESI): m/z [M + H⁺] calcd for C₂₇H₂₇ClN₂O₃ 463.1783, found m/z [M + H⁺] 463.1782.

4.10.9. 2-((1-((4-Chloroquinolin-2-yl)methyl)piperidin-4-yl)methyl)-5,6-dimethoxy-2,3-dihydro-1H-inden-1-one (13)

Under nitrogen atmosphere, the compound **12** (0.0600 g; 12.9 mmol) was added in 1.00 mL of anhydrous pyridine and the mixture was stirred for 10 min. After that was added NaBH₄ (0.010 g; 0.264 mmol) in small portions, and let stirred for more 5 min at room temperature. Then, the mixture was heated at 60 °C for 20 min, cooled until 0 °C, and at this point added 3 mL of a HCl (5%) solution and stirred for more 20 min. The mixture was partitioned with dichloromethane. The solvent was removed by reduced pressure, and the crude material was purified by flash chromatography with dichloromethane:ethyl acetate gradient. Yields: 57% (34.6 mg); mp: 159–160 °C. ¹H NMR (400 MHz, CDCl₃): 8.21 (1H, dd, J = 8.4, 0.9 Hz, H-9), 8.07 (1H, d, J = 8.5 Hz, H-6), 7.78 (1H, s, H-3), 7.74 (1H, ddd, J = 8.4, 6.9, 1.4 Hz, H-8), 7.61 (1H, ddd, J = 8.2, 6.9, 1.2 Hz, H-7), 7.17 (1H, s, H-23), 6.86 (1H, s, H-26), 3.96 (3H, s, H-28), 3.90 (3H, s, H-27), 3.79 (2H, s, H-11), 3.25 (1H, dd, J = 17.6, 8.1 Hz, H-19a), 2.93 (2H, t, J = 10.0 Hz, H-12eq, H-16eq), 2.78–2.67 (2H, m, H-19b), 2.16 (2H, t, J = 11.4 Hz, H-12ax, H-16ax), 2.00–1.89 (1H, m, H-17a), 1.83–1.3 (6H, m, H-17b, H-14, H-13ax, H-15ax, H-13eq, H-15eq). ¹³C NMR (101 MHz, CDCl₃) δ: 207.8 (C22), 155.5 (C2, C20),

149.5 (24), 148.8 (25), 148.4 (C10), 143.0 (C5), 130.3 (C8), 129.3 (C21 e C6), 127.1 (C7), 125.6 (C4), 124.0 (C9), 121.1 (C3), 107.4 (C26), 104.4 (C23), 65.2 (C11), 56.2 (C27), 56.1 (C28), 54.3 (C12, C16), 45.5 (C18), 38.7 (C17), 34.3 (C14), 33.3 (C19), 33.1 (C15), 31.8 (C13). HRMS (ESI): m/z [M + H⁺] calcd for C₂₇H₂₉ClN₂O₃ 465.1939 found m/z [M + H⁺] 465.1931.

4.10.10. (E)2-((1-((4-Aminoquinolin-2-yl)methyl)piperidin-4-yl)methylene)-5,6-dimethoxy-2,3-dihydro-1H-inden-1-one (14)

A mixture of [Pd(cinnamyl)Cl]₂ (0.0083 g; 0.0160 mmol) and BippyPhos (0.0273 g; 0.054 mol) in 1.5 mL of anhydrous dioxane, was stirred for 5 min, at room temperature under argon protection. After, was added NaOtBu (0.104 g; 1.08 mmol), and the chloride intermediate **12** (0.080 g; 0.173 mmol), the mixture was stirred until the solubilization of **12**. Then, was dropwise added a solution of dioxane-NH₄OH (0.5 M), followed by heating at 110 °C for 3 h. The solvent was removed by reduced pressure, and the mixture resuspended in dichloromethane, filtered in filter PVDF 30 mm 0.45μ. After, the crude material was purified by flash chromatography with dichloromethane:metanol gradient (0–15%). Yields 16% (0.007 g). ¹H NMR (300 MHz, CDCl₃) δ: 8.21 (1H, d, J = 6.4 Hz, H-9), 7.99 (1H, d, J = 8.3 Hz, H-6), 7.58 (1H, t, J = 7.4 Hz, H-8), 7.4 (1H, t, J = 7.6 Hz, H-7), 7.19 (1H, s, H-26), 6.93 (1H, s, H-3), 6.85 (1H, s, H-23), 6.50 (1H, d, J = 9.4 Hz, H-17), 3.91 (3H, s, H-27), 3.85 (3H, s, H-28), 3.69 (2H, s, H-11), 3.50 (2H, s, H-19), 2.86–2.75 (2H, m, H-12 eq, H-16eq), 2.10–2.30 (3H, m, H-12ax, H-16ax, H-14), 1.66–1.46 (4H, m, H-13ax, H-13ax, H-15eq, H-15ax). ¹³C NMR (75 MHz, CDCl₃) δ: 191.6 (C22), 154.4 (C24), 148.5 (C25), 143.7 (C20), 138.2 (C17), 134.9 (C18), 132.2 (C21), 130.6 (C8), 124.6 (C7), 121.4 (C9), 122.1 (C6), 106.3 (C23), 103.9 (C26), 101.4 (C3), 61.4 (C11), 55.3 (C27), 55.1 (C28), 52.3 (C12 and C16), 35.6 (C14), 30.1 (C13 and C15), 28.7 (C19). HRMS (ESI): m/z [M + H⁺] calcd C₂₇H₂₉N₃O₃ 444.2282 found m/z [M + H⁺] 444.2297.

4.10.11. 2-((1-((4-Aminoquinolin-2-yl)methyl)piperidin-4-yl)methyl)-5,6-dimethoxy-2,3-dihydro-1H-inden-1-one (15)

A mixture of [Pd(cinnamyl)Cl]₂ (0.0083 g; 0.0160 mmol) and BippyPhos (0.0273 g; 0.054 mol) in 1.5 mL of anhydrous dioxane, was stirred for 5 min, at room temperature under argon protection. After, NaOtBu was added to the mixture (104.0 mg; 1.08 mmol), and the chloride intermediate **13** (0.022 g; 0.049 mmol) dissolved in dioxane. Then, was dropwise added a solution of dioxane-NH₄OH (0.5 M), followed by heating at 110 °C for 5 h. The solvent was removed by reduced pressure, and the mixture resuspended in dichloromethane, filtered in filter PVDF 30 mm 0.45μ. After, the crude material was purified by analytical HPLC gradient methanol: H₂O (TFA 0.1%), R_T = 23 min. Yields 9% (0.002 g). ¹H NMR (600 MHz, MeOD-₃mm) δ 8.29 (1H, d, J = 8.4 Hz, H-9), 7.95–7.89 (2H, m, H-6, H-8), 7.70–7.62 (1H, m), 7.15 (1H, s, H-26), 7.07 (1H, s, H-23), 6.88 (1H, s, H-3), 3.94 (3H, s, MeO), 3.86 (5H, s, MeO, H-11), 3.31 (1H, m, H-19a), 3.12–3.00 (2H, m, H-12 eq, H-16eq), 2.84–2.71 (2H, m, H-16, H-19b), 2.43–2.36 (2H, m, H12ax, H16ax), 1.95–1.74 (2H, m, H-13eq, H-15eq), 1.72–1.55 (1H, m, H-14), 1.53–1.33 (2H, m, H-13ax, H15ax). ¹³C NMR (151 MHz, MeOD) δ 210.7 (C22), 160.0 (C4), 157.7 (C24), 151.5 (C24), 150.9 (C21), 140.8 (C10), 135.1 (C8), 129.8 (C20), 127.6 (C7), 124.2 (C9), 121.3 (C6), 117.3 (C5), 108.9 (C23), 105.1 (C3), 102.8 (C26), 60.5 (C11), 56.7 (C28), 56.4 (C27), 54.9 (C12 and C16), 46.5 (C18), 39.6 (C17), 34.0 (C19), 33.5 (C14), 32.2 (C13 and C15). HRMS (ESI): m/z [M + H⁺] calcd C₂₇H₃₁N₃O₃ 446.2438 found m/z [M + H⁺] 446.2414.

Author contributions

^aT.P.C.C. and I.C. performed the organic synthesis of compounds; ^bS.P.M.; ^cF.J.C.; ^dJ.J.B. contributed with the STD-NMR studies; ^eC.R.;

C.R.; V.S.P.; A.M; N.C. performed the molecular modeling experiments; ^eC.P. carried out the AChE inhibition assays; ^cW.O.C.; N.C.S.M.; ^{c,d}E.T.S.H.; C.S.T. performed the SH-SY5Y cells assays; I.C. and A.M. conceived and design the study.

Notes

The authors declare no competing financial interest.

Acknowledgments

Financial support of this research provided by the Fundação de Pesquisa e Amparo do Estado de São Paulo-FAPESP (Proc. 12/04054-5; 12/14114-5; 13/50788-3; 14-10414-0); Coordenação de Aperfeiçoamento de Pessoal de Nível Superior (CAPES), CSIC (grant no. i-LINK-0801), MINECO (grants no. SAF2016-76693-R to A.M., and CTQ2015-64597-C2-1 to J.J.B. and F.J.C.) and MEC (FPU15/1465 to VSP) is acknowledged. A.M. and F.J.C. are members of the “CIB Intramural Program “Molecular Machines for Better Life” (MACBET)“.

Appendix A. Supplementary data

Supplementary data related to this article can be found at <http://dx.doi.org/10.1016/j.ejmech.2017.08.051>.

References

- [1] H. Hippius, G. Neundörfer, The discovery of Alzheimer's disease, *Dialogues Clin. Neurosci.* 5 (2003) 101–108.
- [2] Alzheimer Society: <https://www.alzheimers.org.uk/>. (10.12.2015).
- [3] J. Ramirez-Bermudez, Alzheimer's disease: critical notes on the history of a medical concept, *Arch. Med. Res.* 43 (2012) 595–599.
- [4] [\(09.01.2017\).](https://www.alz.co.uk/research/worldalzheimerreport2016sheet)
- [5] G.T. Grossberg, Cholinesterase inhibitors for the treatment of Alzheimer's disease, *Curr. Ther. Res.* 64 (2003) 216–235.
- [6] A. Martinez, A. Castro, Novel cholinesterase inhibitors as future effective drugs for the treatment of Alzheimer's disease, *Expert Opin. Invest. Drugs* 15 (2006) 1–12.
- [7] K. Kuca, O. Soukup, P. Maresova, J. Korabecny, E. Nepovimova, B. Klimova, J. Honegr, T.C. Ramalho, T.C.C. França, Current approaches against Alzheimer's disease in clinical trials, *J. Braz. Chem. Soc.* 27 (2016) 641–649.
- [8] S.T. Ferreira, M.N.N. Vieira, F.G. De Felice, Soluble protein oligomers as emerging toxins in alzheimer's and other amyloid diseases, *IUBMB Life* 59 (2007) 332–345.
- [9] M.E. Kennedy, A.W. Stamford, X. Chen, K. Cox, J.N. Cumming, M.F. Dockendorf, M. Egan, L. Ereshesky, R.A. Hodgson, L.A. Hyde, S. Jhee, H.J. Kleijn, R. Kuvelkar, W. Li, B.A. Mattson, H. Mei, J. Palcza, J.D. Scott, M. Tanen, M.D. Troyer, J.L. Tseng, J.A. Stone, E.M. Parker, M.S. Forman, The BACE1 inhibitor verubecestat (MK-8931) reduces CNS β-amyloid in animal models and in Alzheimer's disease patients, *Sci. Transl. Med.* 8 (2016), 363ra150–363ra150.
- [10] J. Budni, M.L. Garcez, J.d. Medeiros, E. Cassaro, T. Bellettini-Santos, F. Mina, J. Quevedo, The anti-inflammatory role of minocycline in Alzheimer's disease, *Curr. Alzheimer Res.* 13 (2016) 1319–1329.
- [11] D. Seripa, V. Solfrizzi, B.P. Imbimbo, A. Daniele, A. Santamato, M. Lozupone, G. Zuliani, A. Greco, G. Logroscino, F. Panza, Tau-directed approaches for the treatment of Alzheimer's disease: focus on leuco-methylthioninium, *Expert Rev. Neurother.* 16 (2016) 259–277.
- [12] K. Hochgräfe, A. Sydow, D. Matenia, D. Cadinu, S. Könen, O. Petrova, M. Pickhardt, P. Goll, F. Morellini, E. Mandelkow, E.-M. Mandelkow, Preventive methylene blue treatment preserves cognition in mice expressing full-length pro-aggregant human Tau, *Acta Neuropathol. Commun.* 3 (2015) 25.
- [13] F. Panza, D. Seripa, V. Solfrizzi, B.P. Imbimbo, M. Lozupone, A. Leo, R. Sardone, G. Gagliardi, L. Lofano, B.C. Creanza, P. Bisceglia, A. Daniele, A. Bellomo, A. Greco, G. Logroscino, Emerging drugs to reduce abnormal β-amyloid protein in Alzheimer's disease patients, *Expert Opin. Emerg. Drugs* 21 (2016) 377–391.
- [14] [\(11.01.2017\).](http://www.alzforum.org/news/conference-coverage/clinical-trials-alzheimers-disease)
- [15] S. Oddo, A. Caccamo, L. Tran, M.P. Lambert, C.G. Glabe, W.L. Klein, F.M. LaFerla, Temporal profile of amyloid-beta (Abeta) oligomerization in an *in vivo* model of Alzheimer disease. A link between Abeta and tau pathology, *J. Biol. Chem.* 281 (2006) 1599–1604.
- [16] A.M. Swomley, S. Förster, J.T. Keeney, J. Triplett, Z. Zhang, R. Sultana, D.A. Butterfield, Abeta, oxidative stress in Alzheimer disease: evidence based on proteomics studies, *Biochim. Biophys. Acta Mol. Basis Dis.* 1842 (2014) 1248–1257.
- [17] D.A. Butterfield, A.M. Swomley, R. Sultana, Amyloid β-peptide (1–42)-induced oxidative stress in Alzheimer disease: importance in disease pathogenesis and progression, *Antioxidants Redox Signal.* 19 (2013) 823–835.
- [18] F. Bao, L. Wicklund, P.N. Lacor, W.L. Klein, A. Nordberg, A. Marutle, Different β-amyloid oligomer assemblies in Alzheimer brains correlate with age of disease onset and impaired cholinergic activity, *Neurobiol. Aging* 33 (2012) 825.e1–825.e13.
- [19] K.P. Kepp, Alzheimer's disease due to loss of function: a new synthesis of the available data, *Prog. Neurobiol.* 143 (2016) 36–60.
- [20] N.C. Inestrosa, M.C. Dinamarca, A. Alvarez, Amyloid-cholinesterase interactions. Implications for Alzheimer's disease, *FEBS J.* 275 (2008) 625–632.
- [21] T. Silva, J. Reis, J. Teixeira, F. Borges, Alzheimer's disease, enzyme targets and drug discovery struggles: from natural products to drug prototypes, *Ageing Res. Rev.* 15 (2014) 116–145.
- [22] P. Camps, X. Formosa, C. Galdeano, T. Gómez, D. Muñoz-Torrero, M. Scarpellini, E. Viayna, A. Badia, M.V. Clos, A. Camins, M. Pallás, M. Bartolini, F. Mancini, V. Andrisano, J. Estelrich, M. Lizondo, A. Bidon-Chanal, F.J. Luque, Novel donepezil-based inhibitors of acetyl- and butyrylcholinesterase and acetylcholinesterase-induced β-amyloid aggregation, *J. Med. Chem.* 51 (2008) 3588–3598.
- [23] P. Muñoz-Ruiz, L. Rubio, E. García-Palomero, I. Dorronsoro, M. del Monte-Millán, R. Valenzuela, P. Usán, C. de Austria, M. Bartolini, V. Andrisano, A. Bidon-Chanal, M. Orozco, F.J. Luque, M. Medina, A. Martínez, Design, synthesis, and biological evaluation of dual binding site acetylcholinesterase Inhibitors: new disease-modifying agents for Alzheimer's disease, *J. Med. Chem.* 48 (2005) 7223–7233.
- [24] C. Galdeano, E. Viayna, I. Sola, X. Formosa, P. Camps, A. Badia, M.V. Clos, J. Relat, M. Ratia, M. Bartolini, F. Mancini, V. Andrisano, M. Salmona, C. Minguilón, G.C. González-Muñoz, M.I. Rodríguez-Franco, A. Bidon-Chanal, F.J. Luque, D. Muñoz-Torrero, Huperine–tacrine heterodimers as anti-amyloidogenic compounds of potential interest against Alzheimer's and prion diseases, *J. Med. Chem.* 55 (2012) 661–669.
- [25] M.L. Bolognesi, M. Bartolini, F. Mancini, G. Chiriano, L. Ceccarini, M. Rosini, A. Milelli, V. Tumiatti, V. Andrisano, C. Melchiorre, Bis(7)-tacrine derivatives as multitarget-directed ligands: focus on anticholinesterase and anti-amyloid activities, *ChemMedChem* 5 (2010) 1215–1220.
- [26] J. Cheung, M.J. Rudolph, F. Burshteyn, M.S. Cassidy, E.N. Gary, J. Love, M.C. Franklin, J.J. Height, Structures of human acetylcholinesterase in complex with pharmacologically important ligands, *J. Med. Chem.* 55 (2012) 10282–10286.
- [27] J.S. Lan, T. Zhang, Y. Liu, J. Yang, S.S. Xie, J. Liu, Z.Y. Miao, Y. Ding, Design, synthesis and biological activity of novel donepezil derivatives bearing N-benzyl pyridinium moiety as potent and dual binding site acetylcholinesterase inhibitors, *Eur. J. Med. Chem.* 133 (2017) 184–196.
- [28] C.B. Mishra, S. Kumari, A. Manral, A. Prakash, V. Saini, A.M. Lynn, M. Tiwari, Design, synthesis, *in-silico* and biological evaluation of novel donepezil derivatives as multi-target-directed ligands for the treatment of Alzheimer's disease, *Eur. J. Med. Chem.* 125 (2017) 736–750.
- [29] M. Estrada, C. Herrera-Arozamena, C. Pérez, D. Viña, A. Romero, J.A. Morales-García, A. Pérez-Castillo, M.I. Rodríguez-Franco, New cinnamic – N-benzyl-piperidine and cinnamic – N,N-dibenzyl(N-methyl)amine hybrids as Alzheimer-directed multitarget drugs with antioxidant, cholinergic, neuro-protective and neurogenic properties, *Eur. J. Med. Chem.* 121 (2016) 376–386.
- [30] K.S. Dias, C.T. de Paula, T. Dos Santos, I.N. Souza, M.S. Boni, M.J. Guimaraes, F.M. da Silva, N.G. Castro, G.A. Neves, C.C. Veloso, M.M. Coelho, I.S. de Melo, F.C. Giusti, A. Giusti-Paiva, M.L. da Silva, L.E. Dardenne, I.A. Guedes, L. Pruccoli, F. Morroni, A. Tarozzi, C. Viegas Jr., Design, synthesis and evaluation of novel feruloyl-donepezil hybrids as potential multitarget drugs for the treatment of Alzheimer's disease, *Eur. J. Med. Chem.* 130 (2017) 440–457.
- [31] L. Wang, G. Esteban, M. Ojima, O.M. Bautista-Aguilera, T. Inokuchi, I. Moraleda, I. Iriepa, A. Samadi, M.B. Youdim, A. Romero, E. Soriano, R. Herrero, A.P. Fernandez Fernandez, M. Ricardo Martinez, J.L. Marco-Contelles, M. Unzeta, Donepezil + propargylamine + 8-hydroxyquinoline hybrids as new multifunctional metal-chelators, ChE and MAO inhibitors for the potential treatment of Alzheimer's disease, *Eur. J. Med. Chem.* 80 (2014) 543–561.
- [32] P. Camps, X. Formosa, C. Galdeano, T. Gómez, D. Muñoz-Torrero, L. Ramírez, E. Viayna, E. Gómez, N. Isambert, R. Lavilla, A. Badia, M.V. Clos, M. Bartolini, F. Mancini, V. Andrisano, A. Bidon-Chanal, Ó. Huertas, T. Dafni, F.J. Luque, Tacrine-based dual binding site acetylcholinesterase inhibitors as potential disease-modifying anti-Alzheimer drug candidates, *Chem. Biol. Interact.* 187 (2010) 411–415.
- [33] D. Alonso, I. Dorronsoro, L. Rubio, P. Muñoz, E. García-Palomero, M. Del Monte, A. Bidon-Chanal, M. Orozco, F.J. Luque, A. Castro, M. Medina, A. Martínez, Donepezil–tacrine hybrid related derivatives as new dual binding site inhibitors of AChE, *Bioorg. Med. Chem.* 13 (2005) 6588–6597.
- [34] D. Shao, C. Zou, C. Luo, X. Tang, Y. Li, Synthesis and evaluation of tacrine–E2020 hybrids as acetylcholinesterase inhibitors for the treatment of Alzheimer's disease, *Bioorg. Med. Chem. Lett.* 14 (2004) 4639–4642.
- [35] J. Korabecny, R. Dolezal, P. Cabelova, A. Horova, E. Hruba, J. Ricny, L. Sedlacek, E. Nepovimova, K. Spilovska, M. Andrs, K. Musilek, V. Opletalova, V. Sepsova, D. Ripova, K. Kuca, 7-MEOTA–donepezil like compounds as cholinesterase inhibitors: synthesis, pharmacological evaluation, molecular modeling and QSAR studies, *Eur. J. Med. Chem.* 82 (2014) 426–438.

- [36] L.R. Ferguson, W.A. Denny, Genotoxicity of non-covalent interactions: DNA intercalators, *Mutat. Res./Fund. Mol. Mech. Mutagen.* 623 (2007) 14–23.
- [37] G.R. Hoffmann, S.M. Deschênes, T. Manyin, R.P.P. Fuchs, Mutagenicity of acridines in a reversion assay based on tetracycline resistance in plasmid pBR322 in Escherichia coli, *Mutat. Res./Fund. Mol. Mech. Mutagen.* 351 (1996) 33–43.
- [38] J. Patocka, D. Jun, K. Kuca, Possible role of hydroxylated metabolites of tacrine in drug toxicity and therapy of Alzheimer's disease, *Curr. Drug Metab.* 9 (2008) 332–335.
- [39] A. Marella, O.P. Tanwar, R. Saha, M.R. Ali, S. Srivastava, M. Akhter, M. Shaquiquzzaman, M.M. Alam, Quinoline: a versatile heterocyclic, *Saudi Pharm. J.* 21 (2013) 1–12.
- [40] Z.M. Wang, P. Cai, Q.H. Liu, D.Q. Xu, X.L. Yang, J.J. Wu, L.Y. Kong, X.B. Wang, Rational modification of donepezil as multifunctional acetylcholinesterase inhibitors for the treatment of Alzheimer's disease, *Eur. J. Med. Chem.* 123 (2016) 282–297.
- [41] C.H.T.P. da Silva, V.L. Campo, I. Carvalho, C.A. Taft, Molecular modeling, docking and ADMET studies applied to the design of a novel hybrid for treatment of Alzheimer's disease, *J. Mol. Graph. Model.* 25 (2006) 169–175.
- [42] A.F. Abdel-Magid, C.A. Maryanoff, K.G. Carson, Reductive amination of aldehydes and ketones by using sodium triacetoxyborohydride, *Tetrahedron Lett.* 31 (1990) 5595–5598.
- [43] N. Boyer, P. Gloanec, G. De Nanteuil, P. Jubault, J.-C. Quirion, Synthesis of α,α -difluoro- β -amino esters or gem-difluoro- β -lactams as potential metal-carboxypeptidase inhibitors, *Eur. J. Org. Chem.* 2008 (2008) 4277–4295.
- [44] W. Engen, T.E. O'Brien, B. Kelly, J. Do, L. Rillera, L.K. Stapleton, J.F. Youngren, M.O. Anderson, Synthesis of aryl-heteroaryl ureas (AHUs) based on 4-aminoquinoline and their evaluation against the insulin-like growth factor receptor (IGF-1R), *Bioorg. Med. Chem.* 18 (2010) 5995–6005.
- [45] Y. Tagawa, K. Yamashita, Y. Higuchi, Y. Goto, Improved oxidation of active methyl group of N-heteroaromatic compounds by selenium dioxide in the presence of tert-butyl hydroperoxide, *Heterocycles* 60 (2003) 5.
- [46] D.B. Dess, J.C. Martin, Readily accessible 12-I-5 oxidant for the conversion of primary and secondary alcohols to aldehydes and ketones, *J. Org. Chem.* 48 (1983) 4155–4156.
- [47] I. Carvalho, P. Andrade, V.L. Campo, P.M.M. Guedes, R. Sesti-Costa, J.S. Silva, S. Schenkman, S. Dedola, L. Hill, M. Rejzek, S.A. Nepogodiev, R.A. Field, 'Click chemistry' synthesis of a library of 1,2,3-triazole-substituted galactose derivatives and their evaluation against Trypanosoma cruzi and its cell surface trans-sialidase, *Bioorg. Med. Chem.* 18 (2010) 2412–2427.
- [48] P. Camps, L.R. Domingo, X. Formosa, C. Galdeano, D. González, D. Muñoz-Tornero, S. Segalés, M. Font-Bardia, X. Solans, Highly diastereoselective one-pot synthesis of spiro[cyclopenta[*a*]indene-2,2'-indene]diones from 1-indanones and aromatic aldehydes, *J. Org. Chem.* 71 (2006) 3464–3471.
- [49] R.T. Williamson, B.L. Marquez, W.H. Gerwick, K.E. Kover, One- and two-dimensional gradient-selected HSQMBC NMR experiments for the efficient analysis of long-range heteronuclear coupling constants, *Magn. Reson. Chem.* 38 (2000) 265–273.
- [50] V. Lacerda, G.V.J. da Silva, M.G. Constantino, C.F. Tormena, R.T. Williamson, B.L. Marquez, Long-range JCH heteronuclear coupling constants in cyclopentane derivatives, *Magn. Reson. Chem.* 44 (2006) 95–98.
- [51] V. Lacerda, G.V.J. da Silva, C.F. Tormena, R.T. Williamson, B.L. Marquez, Long-range JCH heteronuclear coupling constants in cyclopentane derivatives. Part II, *Magn. Reson. Chem.* 45 (2007) 82–86.
- [52] V. Lacerda, G.V.J. da Silva, M.G. Constantino, R.B. dos Santos, E.V.R. de Castro, R.C. Silva, Stereochemistry of cyclopentane derivatives from 2, 3JCH dependence on dihedral angle (θ H C C X), *Magn. Reson. Chem.* 46 (2008) 268–273.
- [53] J.R. Mohrig, D.G. Alberg, C.H. Cartwright, M.K.H. Pfum, J.S. Aldrich, J.K. Anderson, S.R. Anderson, R.L. Fimmen, A.K. Snover, Stereochemistry of 1,2-elimination reactions at the E2-E1cB interface-tert-butyl 3-tosyloxybutanoate and its thioester, *Org. Biomol. Chem.* 6 (2008) 1641–1646.
- [54] M. Haring, D. Kuck, The first centrohexaandane bearing twelve functional groups at its outer molecular periphery and related lower veratrole-derived centropolyindanes, *Eur. J. Org. Chem.* 2006 (2006) 1647–1655.
- [55] S.M. Crawford, C.B. Lavery, M. Stradiotto, BippyPhos: a single ligand with unprecedented scope in the Buchwald-Hartwig amination of (hetero)aryl chlorides, *Chemistry* 19 (2013) 16760–16771.
- [56] G.L. Ellman, K.D. Courtney, V. Andres, R.M. Featherstone, A new and rapid colorimetric determination of acetylcholinesterase activity, *Biochem. Pharmacol.* 7 (1961) 88.
- [57] B. Meyer, T. Peters, NMR spectroscopy techniques for screening and identifying ligand binding to protein receptors, *Angew. Chem. Int. Ed. Engl.* 42 (2003) 864–890.
- [58] Y.S. Wang, D. Liu, D.F. Wyss, Competition STD NMR for the detection of high-affinity ligands and NMR-based screening, *Magn. Reson. Chem.* 42 (2004) 485–489.
- [59] F. Marcelo, C. Dias, A. Martins, P.J. Madeira, T. Jorge, M.H. Florencio, F.J. Canada, E.J. Cabrita, J. Jimenez-Barbero, A.P. Rauter, Molecular recognition of rosmarinic acid from *Salvia sclarea* extracts by acetylcholinesterase: a new binding site detected by NMR spectroscopy, *Chemistry* 19 (2013) 6641–6649.
- [60] C. Airoldi, E. Sironi, C. Dias, F. Marcelo, A. Martins, A.P. Rauter, F. Nicotra, J. Jimenez-Barbero, Natural compounds against Alzheimer's disease: molecular recognition of Abeta1-42 peptide by *Salvia sclarea* extract and its major component, rosmarinic acid, as investigated by NMR, *Chem. Asian J.* 8 (2013) 596–602.
- [61] A. Viegas, J. Manso, M.C. Corvo, M.M. Marques, E.J. Cabrita, Binding of ibuprofen, ketorolac, and diclofenac to COX-1 and COX-2 studied by saturation transfer difference NMR, *J. Med. Chem.* 54 (2011) 8555–8562.
- [62] K.W. Borrelli, A. Vitalis, R. Alcantara, V. Guallar, PELE: protein energy landscape exploration. A novel Monte Carlo based technique, *J. Chem. Theory Comput.* 1 (2005) 1304–1311.
- [63] H.M. Berman, J. Westbrook, Z. Feng, G. Gilliland, T.N. Bhat, H. Weissig, I.N. Shindyalov, P.E. Bourne, The protein data bank, *Nucleic Acids Res.* 28 (2000) 235–242.
- [64] Roca C., Requena C., Sebastian V., Malhora S., Pérez C., Martínez A., Páez J.A. and Campillo, N.E., AChE, an old well-known enzyme with new allosteric sites: discovery of allosteric modulators, *J. Chem. Inf. Mol. Model.*, (submitted for publication).
- [65] G.M. Morris, R. Huey, W. Lindstrom, M.F. Sanner, R.K. Belew, D.S. Goodsell, A.J. Olson, AutoDock4 and AutoDockTools4: automated docking with selective receptor flexibility, *J. Comput. Chem.* 30 (2009) 2785–2791.
- [66] B.J. Bennion, S.G. Essiz, E.Y. Lau, J.L. Fattebert, A. Emigh, F.C. Lightstone, A wrench in the works of human acetylcholinesterase: soman induced conformational changes revealed by molecular dynamics simulations, *PLoS One* 10 (2015) e0121092.
- [67] M.C. Franklin, M.J. Rudolph, C. Ginter, M.S. Cassidy, J. Cheung, Structures of paraoxon-inhibited human acetylcholinesterase reveal perturbations of the acyl loop and the dimer interface, *Proteins* 84 (2016) 1246–1256.
- [68] C.J. Tsai, A. del Sol, R. Nussinov, Allostery: absence of a change in shape does not imply that allostery is not at play, *J. Mol. Biol.* 378 (2008) 1–11.
- [69] F.M. Lopes, R. Schroder, M.L. da Frota Jr., A. Zanotto-Filho, C.B. Muller, A.S. Pires, R.T. Meurer, G.D. Colpo, D.P. Gelain, F. Kapczinski, J.C. Moreira, C. Fernandes Mda, F. Klamt, Comparison between proliferative and neuron-like SH-SY5Y cells as an in vitro model for Parkinson disease studies, *Brain Res.* 1337 (2010) 85–94.
- [70] M. Zimmermann, Neuronal AChE splice variants and their non-hydrolytic functions: redefining a target of AChE inhibitors? *Br. J. Pharmacol.* 170 (2013) 953–967.
- [71] S. Greenfield, Discovering and targeting the basic mechanism of neurodegeneration: the role of peptides from the C-terminus of acetylcholinesterase: non-hydrolytic effects of ace: the actions of peptides derived from the C-terminal and their relevance to neurodegeneration, *Chem. Biol. Interact.* 203 (2013) 543–546.
- [72] G. Johnson, C. Swart, Samuel W. Moore, Interaction of acetylcholinesterase with the G4 domain of the laminin $\alpha 1$ -chain, *Biochem. J.* 411 (2008) 507–514.
- [73] F.M. Lopes, L.L. da Motta, M.A. De Bastiani, B.P. Pfaffenseller, B.W. Aguiar, L.F. de Souza, G. Zanatta, D.M. Vargas, P. Schonhofen, G.F. Londero, L.M. de Medeiros, V.N. Freire, A.L. Dafre, M.A. Castro, R.B. Parsons, F. Klamt, Differentiation enhances dopaminergic features, changes redox parameters, and increases dopamine transporter dependency in 6-hydroxydopamine-induced neurotoxicity in SH-SY5Y cells, *Neurotox. Res.* 31 (2017) 545–559.
- [74] A. Kunzler, F. Zeidán-Chuliá, J. Gasparotto, C.S. Girardi, K. Klafke, L.L. Petiz, R.C. Bortolin, D.C. Rostirolla, A. Zanotto-Filho, M.A. de Bittencourt Pasquali, P. Dickson, P. Dunkley, J.C.F. Moreira, D.P. Gelain, Changes in cell cycle and up-regulation of neuronal markers during SH-SY5Y neurodifferentiation by retinoic acid are mediated by reactive species production and oxidative stress, *Mol. Neurobiol.* (2016), <http://dx.doi.org/10.1007/s12035-016-0189-4>.
- [75] Schrödinger Release 2016-1: Schrödinger Suite 2016-1 Protein Preparation Wizard, Epik, Schrödinger, LLC, New York, NY, 2016. Impact, Schrödinger, LLC, New York, NY, 2016; Prime, Schrödinger, LLC, New York, NY, 2016.
- [76] D.A. Case, T.E. Cheatham III, C.L. Simmerling, J. Wang, R.E. Duke, R. Luo, R.C. Walker, W. Zhang, K.M. Merz, B. Roberts, S. Hayik, A. Roitberg, G. Seabra, J. Swails, A.W. Götz, I. Kolossváry, K.F. Wong, P. Paesani, J. Vanicek, R.M. Wolf, J. Liu, X. Wu, S.R. Brozell, T. Steinbrecher, H. Gohlke, Q. Cai, X. Ye, J. Wang, M.-J. Hsieh, G. Cui, D.R. Roe, D.H. Mathews, M.G. Seetin, R. Salomon-Ferrer, C. Sagui, V. Babin, T. Luchko, S. Gusarov, A. Kovalenko, P.A. Kollman, AMBER 12, University of California, San Francisco, 2012, 2012.
- [77] J.A. Maier, C. Martinez, K. Kasavajhala, L. Wickstrom, K.E. Hauser, C. Simmerling, ff14SB: improving the accuracy of protein side chain and backbone parameters from ff99SB, *J. Chem. Theory Comput.* 11 (2015) 3696–3713.
- [78] Gaussian 09, R. A. M. J. F., G. W. Trucks, H. B. Schlegel, G. E. Scuseria, M. A. Robb, J. R. Cheeseman, G. Scalmani, V. Barone, G. A. Petersson, H. Nakatsuji, X. Li, M. Caricato, A. Marenich, J. Bloino, B. G. Janesko, R. Gomperts, B. Mennucci, H. P. Hratchian, J. V. Ortiz, A. F. Izmaylov, J. L. Sonnenberg, D. Williams-Young, F. Ding, F. Lipparini, F. Egidi, J. Goings, B. Peng, A. Petrone, T. Henderson, D. Ranasinghe, V. G. Zakrzewski, J. Gao, N. Rega, G. Zheng, W. Liang, M. Hada, M. Ehara, K. Toyota, R. Fukuda, J. Hasegawa, M. Ishida, T. Nakajima, Y. Honda, O. Kitao, H. Nakai, T. Vreven, K. Throssell, J. A. Montgomery, Jr., J. E. Peralta, F. Ogliaro, M. Bearpark, J. J. Heyd, E. Brothers, K. N. Kudin, V. N. Staroverov, T. Keith, R. Kobayashi, J. Normand, K. Raghavachari, A. Rendell, J. C. Burant, S. S. Iyengar, J. Tomasi, M. Cossi, J. M. Millam, M. Klene, C. Adamo, R. Cammi, J. W. Ochterski, R. L. Martin, K. Morokuma, O. Farkas, J. B. Foresman, and D. J. Fox, Gaussian, Inc., Wallingford CT, 2016, 2016.
- [79] W.L. Jorgensen, J. Chandrasekhar, J.D. Madura, R.W. Impey, M.L. Klein, Comparison of simple potential functions for simulating liquid water, *J. Chem. Phys.* 79 (1983) 926–935.
- [80] R.A. Lippert, K.J. Bowers, R.O. Dror, M.P. Eastwood, B.A. Gregersen, J.L. Klepeis, I. Kolossvary, D.E. Shaw, A common, avoidable source of error in molecular dynamics integrators, *J. Chem. Phys.* 126 (2007) 046101.

- [81] H.J.C. Berendsen, J.P.M. Postma, W.F.v. Gunsteren, A. DiNola, J.R. Haak, Molecular dynamics with coupling to an external bath, *J. Chem. Phys.* 81 (1984) 3684–3690.
- [82] D.R. Roe, T.E. Cheatham, PTRAJ and CPPTRAJ: software for processing and analysis of molecular dynamics trajectory data, *J. Chem. Theory Comput.* 9 (2013) 3084–3095.
- [83] W. Humphrey, A. Dalke, K. Schulten, VMD: visual molecular dynamics, *J. Mol. Graph.* 14 (1996) 33–38.
- [84] T. PJ, XMGRACE, Version 5.1.19, Center for Coastal and Land-Margin Research, Oregon Graduate Institute of Science and Technology, Beaverton, OR, 2005, 2005.
- [85] D.B. Kokh, S. Richter, S. Henrich, P. Czodrowski, F. Rippmann, R.C. Wade, TRAPP: a tool for analysis of transient binding pockets in proteins, *J. Chem. Inf. Model.* 53 (2013) 1235–1252.
- [86] R. Liu, H. Barkhordarian, S. Emadi, C.B. Park, M.R. Sierks, Trehalose differentially inhibits aggregation and neurotoxicity of beta-amyloid 40 and 42, *Neurobiol. Dis.* 20 (2005) 74–81.
- [87] T. Coccini, L. Manzo, V. Bellotti, U. De Simone, Assessment of cellular responses after short- and long-term exposure to silver nanoparticles in human neuroblastoma (SH-SY5Y) and astrocytoma (D384) cells, *Sci. World J.* 2014 (2014) 259765.
- [88] W.O. Castillo, A.F. Aristizabal-Pachon, A.P. de Lima Montaldi, E.T. Sakamoto-Hojo, C.S. Takahashi, Galanthamine decreases genotoxicity and cell death induced by beta-amyloid peptide in SH-SY5Y cell line, *Neurotoxicology* 57 (2016) 291–297.
- [89] X. Liu, X. Wang, J. Lu, Tenuifolioside A promotes neurite outgrowth in PC12 cells via the PI3K/AKT and MEK/ERK/CREB signaling pathways, *Mol. Med. Rep.* 12 (2015) 7637–7642.